DOKUZ EYLÜL UNIVERSITY

GRADUATE SCHOOL OF NATURAL AND APPLIED SCIENCES

GEMMOLOGICAL AND MINERALOGICAL INVESTIGATIONS AND GENESIS OF THE MASSIVE PURPLE JADE FROM THE HARMANCIK-BURSA REGION

by

Yasemin BAŞEVİRGEN

January, 2012

İZMİR

GEMMOLOGICAL AND MINERALOGICAL INVESTIGATIONS AND GENESIS OF THE MASSIVE PURPLE JADE FROM THE HARMANCIK-BURSA REGION

A Thesis Submitted to the
Graduate School of Natural and Applied Sciences of Dokuz Eylül University
In Partial Fulfillment of the Requirements for the Degree of Master of Science
in Natural Building Stones and Gem Stones Program

by
Yasemin BAŞEVİRGEN

January, 2012
İZMİR

M.Sc. THESIS EXAMINATION RESULT FORM

We have read the thesis entitled **"GEMMOLOGICAL AND MINERALOGICAL INVESTIGATIONS AND GENESIS OF THE MASSIVE PURPLE JADE FROM THE HARMANCIK-BURSA REGION"** completed by **YASEMİN BAŞEVİRGEN** under supervision of **ASSOC. PROF. DR. MURAT HATİPOĞLU** and we certify that in our opinion it is fully adequate, in scope and in quality, as a thesis for the degree of Master of Science.

Assoc. Prof. Dr. Murat HATİPOĞLU

Supervisor

Doç. Dr. Tahip GÜNGÖR

(Jury Member)

Prof. Dr. Turgay ONARAN

(Jury Member)

Prof. Dr. Mustafa SABUNCU
Director
Graduate School of Natural and Applied Sciences

ACKNOWLEDGMENTS

First of all, I would like to express my gratefulness and my special thanks to my supervisor Assoc. Prof. Dr. Murat Hatipoğlu, Dokuz Eylül University, for his guidance, patience and support, as well as his understanding. Next, the same compliments to my honorary advisor Dr. Steven S. Chamberlain who is a mineralogy coordinator in the New York State Museum, Centre for Mineralogy Albany, New York, USA. Therefore, I appreciate their time and effort in writing this thesis and greatly value their assistance.

In addition, during the obtaining of the analytical data, I am grateful to Gökhan Gümüş who is the director of the Laboratuary of Batı Anadolu Cement Factory, for X-ray diffraction graphics, to Asst. Yasemin Tuncer-Arslanlar and Prof. Dr. Nurdoğan Can, from Celal Bayar University, for the sharing out of the luminescence spectra, and also to Asst. Prof.Dr. İbrahim Gündoğan and Salim Özcan, from department of Geological Engineering of Dokuz Eylül Üniversity, for preparing and evaluating of the petrographic thin sections.

And of course, I would like to give my endless affection to my family, my husband Enver, and my daughter Yasmin Lara, for their support and encouragement in everything I do. Thank you!

Yasemin BAŞEVİRGEN

GEMMOLOGICAL AND MINERALOGICAL INVESTIGATIONS AND GENESIS OF THE MASSIVE PURPLE JADE FROM THE HARMANCIK-BURSA REGION

ABSTRACT

In the Harmancık-Bursa region of the western Anatolia (Turkey), an extensive contact metamorphic aureole at the border between the Late Mesozoic coherent metaclastic rocks of blueschist facies and the Early Cenozoic intrusive granodiorite stock, hosts a gem material with a mineral assemblage consisting mainly of jadeite, quartz, orthoclase, epidote, chloritoid, and phlogopite minerals. In addition, the chemical analyses show that the mass of the metamorphic aureole has a silica rich calc-alkaline chemical content.

This pale purple-colored material is only found in one narrow provenance in Turkey. Therefore, it is specially called “Turkish (and/or Anatolian) purple jade” on the worldwide gem market. Even though the mineral jadeite is the principal constituent, 40 percent by volume, the material cannot be considered pure jadeite.

Specific gravity value of the jade has unusual. The measured average specific gravity of 3.04 is significantly lower than the normal range for characterized jadeites of 3.24 to 3.43.

Dispersive confocal micro-Raman spectroscopy, as well as the other well-known analytical methods was used to characterize and identify in detail the Turkish purple jade samples. Accordingly, the strong micro-Raman bands that peaked at 1038, 984, 697, 571, 521, 464, 430, 372, 326, 307, 264, and 201 1/cm are characteristics of the Turkish purple jade.

Turkish purple jade samples show numerous broad and intensive luminescence bands. Different luminescence centres produced by cathodoluminescence (CL), radioluminescence (RL), and photoluminescence (PL), and excited by using

irradiation, are due to the overall signals, even though thermoluminescence (TL) sensitivity varies depending on the treatment of the jade samples.

Finally, these parameters provide positive identification with the provenance (geographic origin) of the original Turkish purple jade. It can be seen that the obtained dispersive confocal micro-Raman bands, specific gravity values, luminescence spectra, and trace element contents provide a unique fingerprint for this kind of jadeite-jade gem materials.

Keywords: Purple jadeite-jade, gemmology, specific gravity, dispersive confocal micro-raman spectroscopy, luminescence, Harmancık-Bursa region, Turkey.

HARMANCIK-BURSA BÖLGESİNDEKİ KÜTLESEL MOR JADE'NİN GEMOLOJİK VE MİNERALOJİK İNCELEMELERİ VE OLUŞUM KÖKENİNİN BELİRLENMESİ

ÖZ

Batı Anadolu'da Harmancık-Bursa bölgesinde, Geç Mesozoyik yaşlı düzenli istifsel mavişist fasiyesinin metaklastik kayaları ile Erken Senozoyik yaşlı sokulum yapmış granodiyorit kütlesinin sınırındaki dev boyutlu kontak metamorfik bir hale (dilim), başlıca jadeit, kuvars, ortoklas, epidote, chloritoid ve flogopit minerallerinden meydana gelmiş bir mineral birlikteliğine sahip bir süstaşı malzemesi olarak oluşmuştur. İlaveten, kimyasal analizlere göre, bu metamorfik hale, silisçe zengin bir kalk-alkalen kimyasal içeriğe sahiptir.

Soluk mor renkli eşsiz bu malzeme Türkiye'de sadece bir bölgede bulunur. Bu nedenle, Dünya süstaşı pazarında özel olarak "Türk (ve/veya Anadolu) mor jade"si olarak adlandırılır. Bu jade malzemesinin jadeit mineral içeriği, malzemenin toplamının yüzde 40'ından fazlasına sahip olan ana bileşimsel öge olmasına rağmen, malzeme saf bir jadeit minerali gibi formulüze edilememektedir.

Jade'nin özgül ağırlık değeri aykırıdır. İyi bilinen jadeit-jade'lerin 3.24 den 3.43 e kadar olan değerlerinin aksine, bu jade 3.04'lük bir ortalama özgül ağırlık değerine sahiptir.

Türk mor jade örnekleri, saçınımsal konfokal mikro-Raman spektroskopisi ve de diğer iyi bilinen anlatiksel metotlar kullanarak karakterize etmek ve detaylı tanımlamak için incelenmişlerdir. Buna göre, 1038, 984, 697, 571, 521, 464, 430, 372, 326, 307, 264 ve 201 1/cm'lerde piklenmiş güçlü mikro-Raman bandları, Türk mor jade'sinin karekterisitkleridir.

Türk mor jade örnekleri çok sayıda geniş ve şiddetli lüminesans bandları gösterirler. Radyasyon ışıması kullanılarak uyartılmış katadoluminesans (CL), radyoluminesans (RL) ve fotoluminesans (PL) tarafından üretilen farklı lüninesans

merkezleri, termolüminesans (TL) hassasiyetinin jade örneklerinin ısıl muamelesine bağlı olarak değişmesine rağmen, üst üste binmiş sinyaller yüzünden oluşur.

Sonuç olarak, bu parametreler orijinal Türk jade'nin coğrafik oluşum kökeniyle ilgili kesin veriler sağlamaktadır. Görülmektedir ki, elde edilen saçınımsal konfokal mikro-Raman bandları, özgül ağırlık değerleri, lüminesans grafikleri ve iz element içerikleri bu cins jadeit-jade türü süstaşı için özgün anahtar işaretler vermektedir.

Anahtar sözcükler: Mor jadeit-jade, gemoloji, özgül ağırlık, saçınımsal konfokal mikro-raman spektroskopisi, lüminesans, Harmancık-Bursa bölgesi, Türkiye.

CONTENTS

Page

CHAPTER ONE
INTRODUCTION

1.1 Nomenclature of Jade

The jade as a material is known in many fine nuances of green, but also in shades of white, black, gray, yellow, and orange. However, it is known as rare in laverder and also as the rarest in pale purple colorations. Moreover, all kinds of natural gem-quality jades, either jadeite-jade or nephrite-jade, are extremely rare and highly valued (Harlow and Sorensen, 2005; Harlow et al., 2007).

The word “jade” is derived from the Spanish term ‘piedra de ijada’. Since, when the Spanish conquered Mexico, they saw that people in Mexico powdered jadeite and sometimes mixed it with water for making a cure against numerous internal diseases. The first recorded use of this term is by Nicol Monardes in a work on medicinal plants of the New World written in 1565 (Crowhurst, 2001; Easby, 1991). The term "jade" as used in the gem trade, in fact, refers to two minerals; jadeite (pyroxene group) ($Na(Al,Fe)Si_2O_6$) and nephrite (amphibole group) [$Ca_2(Mg, Fe)_5Si_8O_{22}(OH)_2$] (Prewitt and Burnham, 1966; Cameron and Papike, 1981; Morimoto, 1988 and 1989; Htein and Naing, 1994). However, jadeite is different in chemical composition from nephrite, and can exhibit highly saturated colors and a higher degree of translucency, a higher hardness, and a glassy appearance (Harder, 1995). Because of its superior features, jadeite quickly replaced nephrite as the "jade" of choice among art and gem collectors. Contemporary descriptions of "imperial" jadeite cite the following qualitative attributes; a very intense and uniform green color ranging from "apple green" to "spinach green"; a high degree of uniform translucency; and an extremely smooth finish with a greasy feel and lustre (Nassau and Shigley, 1987; Zhao et al., 1994; Nestola et al., 2007; Bersani and Lottici, 2008).

1.2 History of Jade

Before the 18th century, only nephrites had been found, mined, and carved into art objects or jewellery. During the 1700's, green and/or white colored jadeites were found worldwide localities. Instead of nephrite, jadeite is closely associated with two ancient civilizations, those of Mesoamerica (Mexico, Guatemala, and Belize) and China. Therefore, jadeite material was also used by most of the major civilizations in ancient Mesoamerica; the Olmec, Aztec, Maya, and so forth. Also, this gem, "royal gem" in China, was used in prehistoric times as an ideal tough material for weapons and tools (Andrews, 1986; Easby, 1991, Middleton and Freestone, 1995).

The cut and polished jadeites as loose stones and/or mounted stones on historic and archaeological artifacts have been extracted from the various archaeological excavations in Europe and Turkey so far. However, the reported being in existence of the rough green jadeite occurrences (deposits) in Europe and Turkey are very rare. The Western Alps and Austria in Europe appear to be the main source of jadeite mineral and jadeite-jade material (with including the some other minerals) (Bishop et al., 1977; Biino and Compagnoni, 1992; Adamo et al., 2006; Crowhurst, 2001; Harlow et al., 2007; Teixeira et al., 2010). However, purple colored jade material has been only found in one location in Turkey during the 1970s (Figures 1.1A and 1.1B, Figure 1.2). Preliminary and then detailed investigations of the geological studies comprising the Harmancık-Bursa region reveal that these massive material mass (Figure 1.1C) belongs to a metamorphic zone in the border between a Late Mesozoic aged coherent blueschist metamorphic sequence and an Early Cenozoic aged intrusive granodiorite (Okay, 1980, 1984; 1997 and 2002; Okay and Kelley, 1994; and Okay et al., 1998). Some tons of the material have been commercially exploited, and exported with a specific name as "Turkish (and/or Turkish purple jade" since the 1980s. Therefore, the many polished purple jade gem objects and also rough gemstone specimens (Figures 1.1D and 1.1E) have already been preserved in museums and private collections around the world, that their origin is acknowledged to be only the deposit in the Harmancık-Bursa region of Turkey (Hatipoğlu, 2010; Tuncer-Arslanlar et al., 2011).

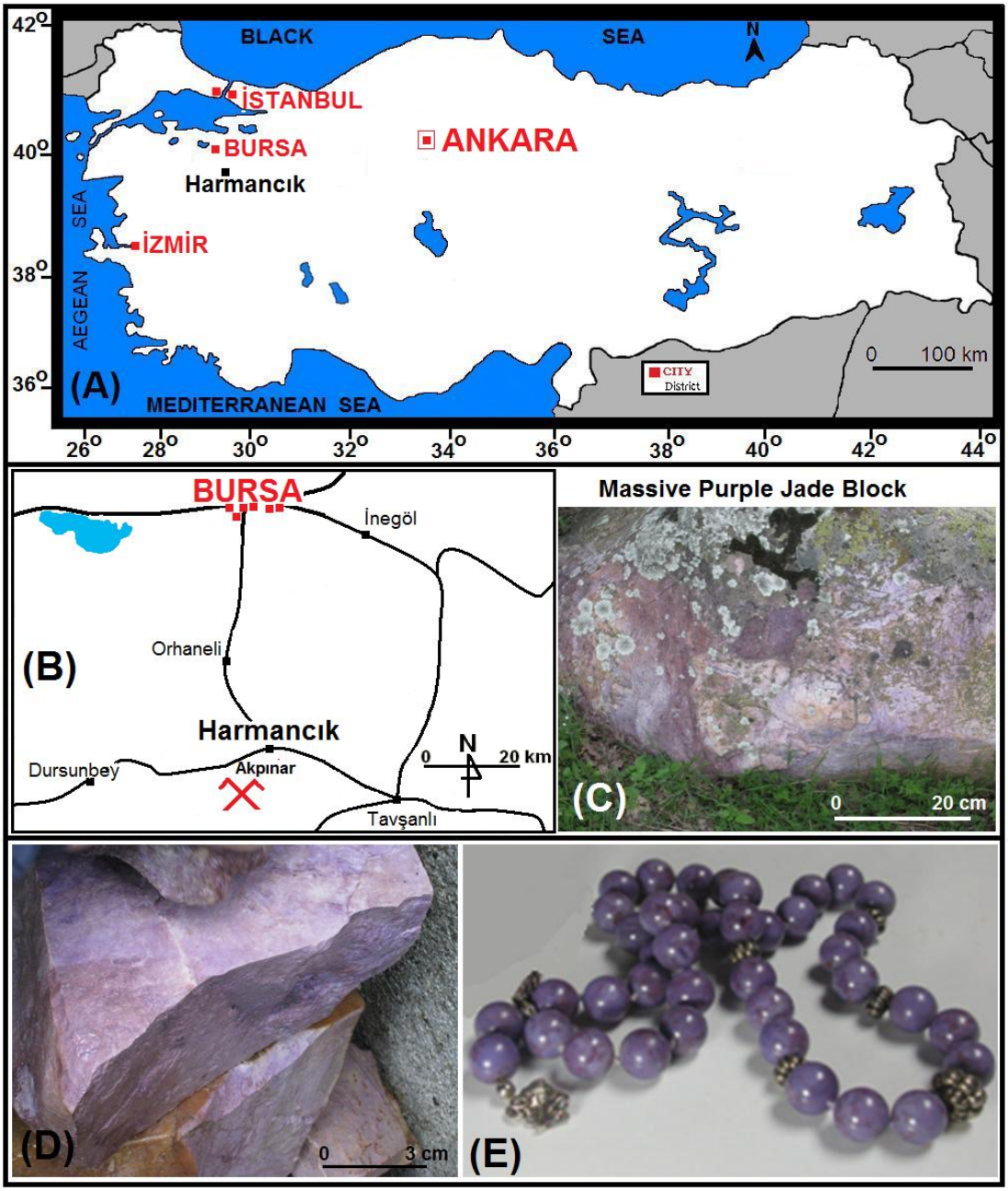

Figure 1.1 Location maps **(A)** and **(B),** showing the Harmancık-Bursa region in Turkey. The fine-grained Turkish purple jade material is found as giant blocks in the field **(C)**. Large-broken rough fragments of gem-quality purple jade rough are the most valuable on the worldwide gem market **(D)**. Cut and polished gem jade objects are widely used as prayer beads with silver parts (totally 112-gr) in Turkey **(E)**.

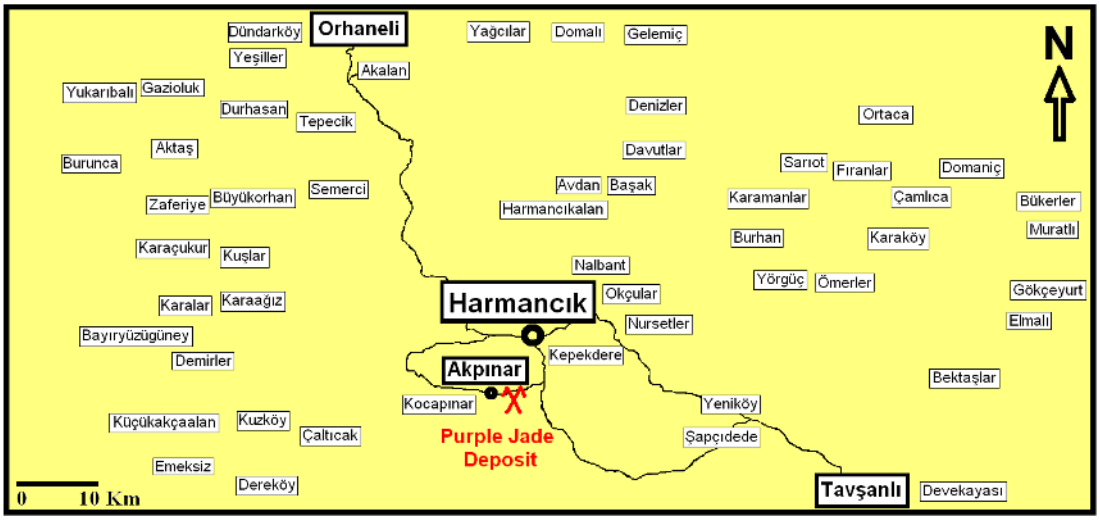

Figure 1.2 Enlarged location map of the Akpınar-Harmancık region comprising the purple jade deposit between the districts of Orhaneli (Bursa) and Tavşanlı (Kütahya).

1.3 Advantage of Spectroscopical Methods in Gemstone Investigation

Since FT-Raman and/or dispersive (Vis)-Raman vibrational bands were first discovered in the 1920s (Raman and Krishnan, 1928), Raman spectrometres have attracted attention in industrial and academical researches. The micro-Raman spectroscopy is a non-destructive and non-invasive investigation technique in principles of high speed and accuracy. In addition, It can also be used for finite-precision analysis in combination with microscopy (Gouadec and Colomban, 2007; Colomban and Prinsloo, 2009; Fan et al., 2009). The frequency wavenumber of the Raman scattering signal is a reflection of the vibration and rotational modes of the molecule (Lewis and Edwards, 2001; Slodczyk and Colomban, 2010; Vandenabeele, 2010). Raman maps are images generated from automated recordings of spectra at discrete points of the sample. They show the variation of any fitted parameter (i.e. intensity, width or position of one band) as a function of the point of analysis. If the mapping is regular and sufficiently tight, one gets a ‘‘smart map’’ of the parameter (color or contrast scaling) superimposed with the optical image of the probed area. Raman mapping is not to be mistaken for direct Raman imaging where a large area of the sample is probed all at once and no fitting is required. More precisely, only photons from a narrow spectral domain are sent to the CCD mosaic and each pixel receives those coming from a given area of the sample. The intensity of the signal thus reveals the presence and location of any substance with a strong Raman signal

in the selected spectral window (Gouadec and Colomban, 2007; Colomban, and Prinsloo, 2009). Hänni et al. (1997) reported some important studies on the gemmological applications of Raman spectroscopy. They showed that the Raman systems used so far were working with a microscope to analyse the surface or sub-surface of materials in the confocal mode. The analytical method, thus, analysed the host gemstone, mineral inclusions or organic fillers for hiding fissures. In addition, databases with Raman spectra of gemstones have been published by Delé-Dubois et al. (1986) in the literary, and also RRUFF (2011) on the internet.

What causes luminescence is a radiation which is emitted when an electron in the structure falls from a high energy level to a lower one. If the crystal dissipates some of the energy as heat, the radiation emitted has a lower energy than the radiation absorbed. Hence the crystal emits light (Blasse and Grabmaier, 1994; Gaft, 2005; Handerson and Imbusch, 2006). Therefore, it can be summarized that (1) a luminescence encodes the defects that exist in all solid materials, (2) all kinds of minerals show many different types of luminescence relating to the many types of the defects (chemical impurities and structural imperfections) they contain, (3) changing the excitation and temperature gives us insights into causes of mineral and/or material luminescence.

Firstly, photoluminescence (PL) is the emission of light from a mineral and/or material when exited by ultraviolet beams. Photoluminescence spectroscopy is a non-contact and non-destructive method of probing the electronic structure of materials. In essence, when the light is directed onto a sample, a process called photo-excitation can occur, where it is absorbed. The photo-excitation causes the material to jump to a higher electronic state, and will then release energy, (photons) as it relaxes and returns to back to a lower energy level. The emission of light or luminescence through this process is photoluminescence (Blasse and Grabmaier, 1994; Gaft et al., 2005; Handerson and Imbusch, 2006). PL (UV-ray induced luminescence) investigations can be used to characterize a variety of material parameters. PL spectroscopy provides electrical (as opposed to mechanical) characterization, and it is a selective and extremely sensitive probe of discrete electronic states. Features of

the emission spectrum can be used to identify surface, interface, and impurity levels and to gauge alloy disorder and interface roughness. The intensity of the PL signal provides information on the quality of surfaces and interfaces (Gfroerer, 2000). Secondly, radioluminescence (RL) (X-ray induced luminescence) is a sensitive technique for studying defects in minerals. X-radiation penetrates and excites the whole volume of the crystal, forming new luminescence defects. RL is stimulated when the samples are excited with ionizing radiation (mainly X-ray) from a radioactive source (Gaft et al., 2005). One of the most suitable methods is that RL light is detected by high-sensitivity wavelength multiplexed TL system (Luff and Townsend, 1993). Thirdly, cathodoluminescence (CL) is an optical and electrical phenomenon in which an electron beam is generated by a cathode ray tube, and then impacts on potentially luminescent centres in a material, giving rise to emission of light. CL (UV-ray induced luminescence) provides essential information on provenance, composition, growth fabrics, diagenetic textures, defects in the lattice, and mineral zonation (Marshall, 1988). Peak-width, peak-position, and transition probability of the luminescence centres are influenced by effects such as interactions within the defects themselves, and interaction between defects and the surrounding crystal lattice. The actual CL color is determined by the number and type of emission and quenching centers present. Superposition of several luminescence bands of different intensities can provide quantitative data on the wavelength and intensity of luminescence and the nature of the luminescence centers (Götze, 2000; Townsend and Rowlands, 2000; Habermann, 2002). Finally, thermoluminescence (TL) glow curves which are created by a heat process have a great importance in identifying the extent of utility of the material to be used in measuring the radiation doses (Melo et al., 2004).

Consequently, some of the analytical methods approach with a non-destructive and non-invasive way during the investigation of a gemstone sample by simply focusing the scope objective focal point to different depths in the sample. Therefore, especially micro-Raman spectroscopy was introduced into the gemmology field in the late twenty century. Moreover, it is becoming more and more important in mineral research, and many related applications have been reported by many

researchers (Gendron and Smith, 2002; Bersani and Lottici, 2008; Fan et al., 2009). Thus, it can be propose that dispersive confocal micro-Raman spectroscopy (DCμRS) is a well-known method for the analyses of gem-minerals. However, DCμRS has not yet been widely used for the purple jade identification and determination.

1.4 Aim and Scope

This study aims: (1) to give geological formation conditions of purple jade gemstone, (2) to establish geographical provenance of the single known mine deposit of purple jade, (3) to indicate trustworthy charecterization parameters for these naturally occurring precious Turkish purple jade, including dispersive confocal micro-Raman vibrational bands, X-ray diffraction pattern, specific gravity value, polarizing microscope images, and major and trace element contents, photoluminescence (PL), radioluminescence (RL), cathodoluminescence (CL), and thermoluminescence (TL) spectra, and thus (4) to permit Turkish purple jade to be able to distinguish from the other natural and synthetic jades and/or color-enhanced jades.

CHAPTER TWO
MATERIALS AND METHODS

2.1 Material

In this study, the investigated purple jade samples were taken from the region near the village of Akpınar in the district of Harmancık of the vicinity of Bursa (Turkey) (Figures 1.1A and 1.1B, Figure 1.2). Even though jades with green and white color deposited in many worldwide localities have been known since ancient times, no location with a large deposit including gem-quality purple jade has been reported in the literature before. Therefore, the world's only known supply of purple jade is found in the region where geologically investigated in this study. The most typical rough blocks (Figure 1.1C) of the purple jade material are obtained from the currently unexploited field in the Akpınar area in this region. The massive material (Figure 1.1D), fine-grained rather than coarsely crystalline, is very suitable for cutting into various gem objects (Figure 1.1E).

2.2 Instrumental Methods

The specific gravity (SG) values of the many purple jade samples were measured using a SG kit and very sensitive electronic balance (measurement sensitivity of 0.001), and were acquired to be based on the formula ($SG = W_{air} / W_{air} - W_{water}$). The test was performed in the DGL-Gemmological Testing Laboratory at Dokuz Eylül University.

The base building components of the purple jade samples were detected by X-ray powder diffraction pattern analysis, using a Cubi-XRD device with a Cu tube and a graphic monochromotor. The representative samples were analyzed with Cu radiation and a 0.3 mm collimator at atmospheric pressure for 10 minutes each, in the range between 5 and 70 (^{o}2-theta). The d-spacing [Å] diffraction matchings of the constituent minerals obtained using the comparative matching technique is based on the positions of peaks with relative intensities [$\%(I/I_o) \geq 4$], 2-theta values below 70

deg., and a tolerance range of ±0.01 (Table 3.1). X-ray powder diffraction patterns were taken in the Research Laboratory of the Batı Anadolu Cement Factory in İzmir (Turkey).

Polarizing microscope images with x4 (a combined magnification of x0.4 objective and x10 ocular), x10 (a combined magnification of x1 objective and x10 ocular) and x40 (a combined magnification of x1 objective and x40 ocular) magnifications under crossed nicols (+N) (active polarizer and analyzer) of the purple jade samples were observed from thin sections using an Olympus BX41 binocular polarizing microscope with a high-intensity 6V, 30W halogen light source combined with a U-CPA and U-OPA optical systems in the Microscopy Laboratory of the Department of Geology at Dokuz Eylül University.

Chemical analyses of the purple jade samples were performed using X-ray fluorescence (XRF) for major oxides and inductively coupled plasma-atomic emission spectroscopy (ICP-AES) for trace elements, as well as WST-SIM to determine ignition losses. These analyses were certified with the code number "IZ10041271", under contract by the accredited ALS Chemex Laboratory in Canada.

The dispersive confocal micro-Raman spectroscopy of the purple jade samples were performed on a dark background at room temperature using a HORIBA Jobin Yvan Scientific XPLORA dispersive confocal micro-Raman spectrometer (DCμRS) with a high throughput integrated spectrograph. The spectrometer uses one laser excitation of about 532 nm. Spectral characteristics are displayed on spectra. Operating temperature is between 15 and 28 ^{o}C. Spectral manipulation as baseline adjustment was carried out using the software of the device. The Raman record was carried out in the DGL-Gemmological Testing Laboratory at Dokuz Eylül University.

Photoluminescence (3D-PL) morphologies of the representative Turkish jade samples were obtained using a Fluorolog 2T Fluorescence Spectrometer. A Xe-lamp with a wavelength range of approximately 370 to 850 nm and with a temperature

range of approximately 230 to 330 K was used as excitation. Luminescence can either be after excitation (where the primary beam has higher energy that the secondary light) or stimulation (where the primary beam has less energy that the luminescence). These wavelengths were selected using a monochromator (Spex 1681 0.22 mm) and emission analysed with a Spex 1680 Double Spectrometer. The detector is front-illuminated open-electrode CCD (200-1100 nm). Finally, the photoluminescence (3D-PL) images of the samples were originally taken by Axum 5.0 software. Latter, the 3D-PL morphology was generated into a counter map as 2D-PL by Surfer 8.0 software. Next, many 2D-PL graphics were produced from the 3D-PL morphology by Surfer 8.0 and Grapher 8.4 softwares.

Radioluminescence (3-D RL) morphologies of the representative Turkish jade samples were performed on a high-sensitivity wavelength multiplexed system with *f*/2.2 optics, which is capable of detection between 200 and 800 nm with a spectral resolution of about 4 nm. The detection range is spanned by two imaging photomultiplier tubes giving 200-440 nm and 380-800 nm coverage, with wavelength dispersion being achieved by grating spectrometers blazed for each region. Radioluminescence morphology was conducted in the range between 25 and 280 K. The measurement was performed using sample stage controlled by Eurotherm controllers from 25 to 280 K whilst heating at 6 K/min. The in-situ irradiation is done using a Philips X-ray tube, typically set to deliver a dose rate of 20 Gy/min (X-ray operating conditions of 30 kV, 10 mA).

Cathodoluminescence (CL) spectra of the representative Turkish jade samples were taken using the 14 keV electrons at the current densities of 0.4 μAcm^{-2} at the temperatures of 77 K and 300 K, respectively. The primary electron beam is normally pulsed using a Thandor TG501 5 MHz function generator as a function with a frequency of 90 Hz, except for the lifetime measurement. The light coming from the samples was focused via a quartz lens onto the entrance slit of a grating monochromator with f/4 light collection, and detected with a blue-sensitive photomultiplier tube (PMT, EMI 9813Q). The quantum efficiency of EMI 9813Q is between 15% and 25% in the range of 250 nm to 800 nm. Two different

measurements can be performed on the samples, using the alternating current (AC) and the direct current (DC), generated in the system. DC measurements can potentially record optical signals from the electron gun source, but this is rejected in the AC operating mode. However, it was only used Alternating Current (AC) measurements on the samples at the room temperature during the experiment. In AC measurement, an Ortholoc-SC9505 two phase lock-in amplifier was employed. This instrument was used in normal mode where it performs in exactly the same way as an ordinary lock-in amplifier, i.e. only one channel is needed. The spectral lines obtained using a mercury (Hg) discharge lamp and He-Ne laser have been used in the wavelength calibration using 3 mm entrance and exit slits on the monochromator. The wavelengths of the spectral lines used in the calibration are 405, 436, 546 and 577 nm for Hg and 633 nm for He-Ne laser. The efficiency of the spectral response of the whole system was obtained by recording the spectrum of a tungsten lamp used with same aperture as in the wavelength calibration. Hence it was possible to correct the wavelength dependent sensitivity of the system. The electron beams were chopped at frequencies from 9 to 900 Hz, and the photomultiplier output were measured on a lock-in amplifier. The wavelength resolution was set at 5 nm for the CL measurements. Since the changes in ion beam energy, the current density may modify the emission spectra and intensity.

Thermoluminescence (TL) glow curves of the representative Turkish jade samples were recorded using a computer controlled thermoluminescence dosimeter reader of Harshaw 3500 with a linear heating rate of 2 Cs^{-1} in N_2 atmosphere at the temperatures ranging from 50 to 400 ^{o}C. The jade samples were irradiated at 300 K for 5 minutes. Irradiation is performed by a Machlett OEG-50A an X-ray tube adjusted to 30 kV and 15 mA. The used filter is Schott KG1, and the measurements were taken immediately after irradiation under the red light in order to overcome any fading effects which influence the glow curves.

CHAPTER THREE
RESULTS AND DISCUSSION

3.1 Provenance and Geological Setting

In this study, the geology of the region around the deposit of purple jade was re-investigated, taking into account previous field observations.

During the geological field investigation, it was noted that the Harmancık-Bursa region displays, in large scale, the complex geological formations belonging to two different continental crusts (Sakarya Continent on the North and Anatolide-Toride Block on the South) separated with the Tethyan Ocean during the Mesozoic Period. At the beginning of Tertiary, after these two terrestrial blocks had been collided, the region was tectonically affected with the Late Alpine Orogenesis (Şengör and Yılmaz, 1981; Bingöl et al., 1982; Kaya et al., 1989; Yılmaz et al., 2010).

In this study, the coherent rock units called the Tavşanlı Zone are of particular interest, since these rock units contain the purple jade material that is the main subject of this thesis. The Tavşanlı Zone constitutes one of the largest and best preserved glaucophane-lawsonite blueschist belts in the world. The Cretaceous blueschists became tectonically overlain by a Cretaceous oceanic accretionary complex and ophiolite. The suture separating the two zones is represented by a major strike-slip fault (Okay, 1980, 1984, 1997 and 2002; Okay and Kelley, 1994, and Okay et al., 1998). Accordingly, the region lying from the north-western (Orhaneli-Bursa) to the south-eastern (Tavşanlı-Kütahya) is mainly covered with a blueschist metamorphic complex sequence that is south of the main Neo-Tethyan suture (Kaya et al., 1989; Okay et al., 1998). Overall, the region represents a subducted former continental crust now present as a blueschist terrain in the orogenic belt.

However, in order to simplify, all geological units can be collected under three main groups: (1) blueschist metaclastic rocks; (2) a granodiorite, and (3) a sedimentary-volcanic sequence. The unique purple gem material occurs in an

extensive contact metamorphic aureole at the border between the blueschist metaclastic rocks and the intrusive granodiorite stock (Figure 3.1). Note that the first and second units have been lumped into the well-known Tavşanlı Zone by many authors (Şengör and Yılmaz, 1981; Bingöl et al., 1982; Okay, 1997 and 2002; Yılmaz et al., 2010).

In the previously published studies, two important geological aspects - age and depositional features - have been determined in the region (Kaya et al., 1989; Okay and Kelley, 1994). First, phengite Rb–Sr and Ar–Ar data from some rocks of the blueschist metaclastic rocks indicate that the complex has been aged as Late Cretaceous (80±5 Mya) for the high pressure/high temperature (HP⁄LT) metamorphism (Sherlock et al., 1999). Secondly, the metamorphic complex has been separated into two main sequences, divided by a tectonic unconformity; the first sequence consists of metapelitic schists at the bottom, marbles in the middle, and a series of metabasites, metacherts, and phyllites at the top (Okay, 1980 and 1984). The overlaying second sequence consists of basalts, radiolarian cherts, and pelagic shales (Okay, 1997 and 2002; Sherlock et al., 1999). Okay (2002) has stated that the Tavşanlı Zone constitutes one of the largest and best preserved glaucophane-lawsonite blueschist belts in the world, with regional distribution of jadeite, lawsonite and glaucophane. Specially, the blueschist metapelites in the zone have jadeite, lawsonite, chloritoid and glaucophane. Therefore, purple jades comprise jadeite, K-feldspar and lawsonite.

3.2 Mineralogical Implications

Similar paragenesis including jadeite crystallization has been reported in the many previously published papers so far.

In the case of USA; the pyroxenes in the blueschist facies of California without jadeites has been reported by Coleman and Clark (1968). Moreover, Coleman (1961) has studied jadeite deposits of the Clear Creek area, New Idria district, San Benito County, California and also, Coleman and Lee (1963) have investigated the

glaucophane-bearing metamorphic rock types of the Cazedero area, California. However, Brothers and Grapes (1989) have studied the structural and chemical variations in pyroxenes to find out which conditions caused jadeite crystallization, and reported the clastic lawsonite, glaucophane, and jadeite pyroxene in Franciscan metagraywackes from the Diablo Range, California. In addition, the neoblastic jadeitic pyroxene in Franciscan metagraywackes from Pacheco Pass in the central Diablo Range of California has been studied for its implications and metamorphism conditions by Ernst and Banno (1991).

In the case of Japan; Chihara (1971 and 1991) has reported mineralogical and petrographical features of jadeites from the Omni-Kotaki area, central Japan.

In the case of Europe; jadeite-bearing metagranites in Mount Mucrone area, Sesiap Lanzo Zone, western Italian Alps have been studied in detail by Compagnoni and Maffeo (1973). In addition, D'Amico and his colleagues (1995) have stated the eclogites and jades as prehistoric implements in Europe, as a case of petrology applied to cultural heritage. Essene (1969) has reported that relatively pure jadeite occurs in the siliceous Corsican gneiss.

This metamorphic sequence of the Tavşanlı Zone was, then, cut by two large granodioritic intrusive bodies (Bingöl et al., 1982) called Orhaneli and Topuk stocks (Okay, 2002). These consist of quartz, plagioclases, orthoclase, hornblendes, and biotite, and belong to the Tavşanlı Zone as well. Dating based on the Ar-Ar technique of the granodiorites (Okay, 1997) has indicated that the stocks were introduced upwards the blueschist metaclastic rocks during the Early and Middle Paleogene (Paleocene and Eocene) Period (65 to 37.8 Mya) of Tertiary. In addition, analysis of the hornblende mineral varieties indicates that the intrusive originate from about 10 km dept below the current topography in the region (Bingöl et al., 1982; Okay, 1984 and 2002). Since the granodiorite stocks do not show detectable deformation structures, their upward intrusion into the blueschist metaclastic rocks must have occurred after the collision of two blocks from two sides of the Tethyan Ocean in the Early Paleogene Period.

During the Late Paleogene (Oligocene) Period (37.8 to 23 Mya) of Tertiary, an extensive contact metamorphic aureole having a silica rich calc-alkaline chemical content (Table 3.2) formed at the border between the blueschist metaclastic rocks and the introduced granodiorite stock occur. This secondary contact metamorphic aureoletic mass is the host rock for the interesting and unique gem material called the "Turkish purple jade" on the worldwide gem market. This aureoletic zone has also a mineral assemblage consisting mainly of jadeite, quartz, orthoclase, epidote, chloritoid, and phlogopite according to X-ray diffraction pattern (Figure 3.1) and polarized-light microscope images (Figures 3.2 and 3.3). X-ray diffractometry (XRD) is used to identify the mineral assemble in the heterogeneous purple jade mass. Accordingly, numerical data (Table 3.1) obtained from XRD analysis of the representative Turkish purple jade sample were matched to those of the base building minerals of the metamorphic aureoletic zone using a comparative matching technique. These mineral components were labelled to aid the readers as quartz, jadeite, orthoclase, epidote, chloritoid, and phlogopite on the X-ray diffraction pattern (Figure 3.1). The ideal XRD data of these minerals for comparison to the investigated samples were compiled from some important crystal structure databases (AMSCD, 2011; RRUFF, 2011; WEBMINERAL, 2011). Accordingly, the three (four) important peak values of these components are as follows;

*3.34(100), 4.26(22), 1.82(14) for quartz [SiO_2],

*2.83(100), 2.42(90), 2.92(80) for jadeite [NaAl (Si_2O_6)] (member of the clinopyroxene group)

*3.18(100), 4.02(90), 3.80(80) for orthoclase [$KAlSi_3O_8$] (member of the feldspar group)

*2.91(100), 2.55(50), 3.49(44) for epidote [$CaPbSrMn^{2+}Al_2Fe^{3+}(SiO_4)(Si_2O_7)O(OH)$]

*4.46(100), 2.46(90), 2.40(85), 2.98(80) for chloritoid [$Fe^{2+}MgMn^{2+}Al_4Si_2O_{10}(OH)_4$]

*9.99(100), 2.61(53), 5.00(30) for phlogopite [$KMg_3AlSi_3O_{10}F(OH)$] (member of the mica group).

However, the positions of peaks with d-spacings [Å] and relative intensities [%(I/I_o)] are labelled for ≥ 4% of 2-theta values below 70 degrees. The labels of overlapped peaks are in order of relative intensities [%(I/I_o)] (Figure 3.1). In addition, it is noted that minor mineral amounts (under 4%) are undetectable by XRD. In this study, the petrographic observations of thin sections of the Turkish purple jade with a polarized-light microscope (Figures. 3.2 and 3.3) show that at least 40% of the gem material of the contact metamorphic aureole consists of jadeite crystallization with high relief and dark greenish-grey color. In some places, jadeite comprises more than 60% of the volume. The other major mineral species are quartz, orthoclase, epidote, chloritoid, and phlogopite, along with some opaque minerals. The analyses of chemical bulk and trace element are consistent with such a mineral paragenesis, especially higher Mn, Na, Ca, and K contents (Table 3.2). As a result, these purple-colored masses should not be considered as pure, fine-grained purple jadeite.

Okay (1980, 1984, and 1997) reported that the jadeite content in thin sections ranges from 34% to 85% and the K-feldspar content from 43% to none; in general, the higher the percentage of jadeite, the lower the percentage of K-feldspars.

Turkish purple jade is found as massive fine-grained blocks. They have an opaque appearance and generally a pale purple color (Figures 1.1C and 1.1D). In spite of this unique pale purple coloration of the masses, some parts of the samples display whitish (quartz-rich portions and veins) and/or yellowish (quartz and orthoclase-rich portions and veins) colorations. Therefore, it can be assumed that in these parts of the samples, the abundance of jadeite is relatively lower.

Finally, a sedimentary and volcanic sequence with many fragments of the debris flows is unconformably settled down at the top of the region. The sequence has been dated as Neogene Period (23 to 3.5 Mya) in many previously published papers (Sherlock et al., 1999; Okay, 2002; Yılmaz et al., 2010).

Table 3.1 Numerical data obtained from XRD analysis of the representative Turkish purple jade sample.

CUBI-XRD

Sample identification: MO251110
Data measured at: 25-Nov-2010

Tube anode: Cu
Wavelength Alpha1 [Å]: 1.54056
Wavelength Alpha2 [Å]: 1.54439

Start angle [°2θ]: 5.015
End angle [°2θ]: 70.025
Maximum intensity: 7551.610
Intensities converted to: FIXED

Number of peaks: 66

Angle [°2θ]	d-value α1 [Å]	d-value α2 [Å]	Peak width [°2θ]	Peak int [counts]	Back. int [counts]	Rel. int [%]	Signif.
8.845	9.9893	10.0141	0.120	2162	331	28.6	5.99
13.890	6.3703	6.3862	0.090	130	174	1.7	1.01
14.235	6.2167	6.2322	0.150	154	166	2.0	1.86
17.740	4.9956	5.0080	0.120	557	130	7.4	3.30
19.910	4.4557	4.4668	0.150	346	114	4.6	2.03
20.850	4.2569	4.2675	0.120	1467	108	19.4	7.91
22.635	4.1042	4.1144	0.090	88	104	1.2	0.88
22.935	3.8744	3.8840	0.150	231	98	3.1	2.63
23.855	3.7270	3.7363	0.120	269	94	3.6	1.87
25.525	3.4868	3.4955	0.180	339	86	4.5	5.49
26.640	3.3434	3.3517	0.150	7552	83	100.0	31.85
27.400	3.2523	3.2604	0.090	154	81	2.0	2.00
27.890	3.1963	3.2043	0.180	384	79	5.1	5.73
28.740	3.1037	3.1114	0.210	259	77	3.4	8.83
29.895	2.9863	2.9938	0.180	538	74	7.1	6.68
30.565	2.9224	2.9297	0.180	713	72	9.4	9.17
31.245	2.8603	2.8674	0.180	357	71	4.7	1.45
31.575	2.8312	2.8382	0.150	1584	69	21.0	12.89
32.050	2.7903	2.7972	0.180	246	69	3.3	3.90
32.835	2.7254	2.7321	0.120	56	67	0.7	0.90
33.515	2.6716	2.6782	0.150	28	64	0.4	0.99
34.125	2.6252	2.6318	0.180	61	64	0.8	0.85
34.630	2.5881	2.5945	0.180	166	62	2.2	0.82
35.060	2.5573	2.5637	0.300	376	62	5.0	12.22
36.000	2.4927	2.4989	0.210	310	61	4.1	7.27
36.540	2.4571	2.4632	0.150	562	59	7.4	8.09
37.150	2.4181	2.4241	0.180	324	58	4.3	6.71
37.820	2.3768	2.3827	0.240	106	56	1.4	2.27
39.455	2.2820	2.2877	0.150	372	55	4.9	7.15
40.285	2.2369	2.2424	0.180	240	53	3.2	6.11
40.870	2.2062	2.2117	0.180	199	52	2.6	4.31
41.805	2.1590	2.1644	0.180	104	52	1.4	2.92
42.445	2.1279	2.1332	0.180	475	50	6.3	9.22
43.700	2.0697	2.0748	0.180	222	49	2.9	5.09
44.185	2.0481	2.0531	0.120	132	49	1.8	1.22
45.380	1.9969	2.0018	0.180	445	48	5.9	6.51
45.785	1.9801	1.9851	0.090	266	48	3.5	0.80
46.095	1.9675	1.9724	0.180	180	46	2.4	1.07
46.660	1.9450	1.9499	0.180	50	46	0.7	1.29
48.105	1.8899	1.8946	0.210	31	45	0.4	2.10
49.520	1.8392	1.8437	0.120	41	44	0.5	0.80
50.125	1.8184	1.8229	0.180	630	44	8.3	14.63
51.905	1.7601	1.7645	0.180	169	42	2.2	5.11
52.915	1.7289	1.7332	0.300	66	41	0.9	3.18
54.410	1.6849	1.6891	0.240	71	40	0.9	1.38
54.850	1.6724	1.6765	0.120	231	40	3.1	3.20
55.315	1.6594	1.6635	0.120	166	40	2.2	1.10
55.830	1.6453	1.6494	0.300	159	38	2.1	3.30
56.585	1.6252	1.6292	0.180	79	38	1.0	1.63
57.120	1.6112	1.6152	0.240	71	38	0.9	1.16
57.725	1.5957	1.5997	0.180	48	38	0.6	0.97
58.650	1.5728	1.5767	0.210	166	37	2.2	5.05
59.555	1.5510	1.5549	0.240	161	37	2.1	4.48
59.935	1.5421	1.5459	0.090	462	36	6.1	2.36
60.765	1.5230	1.5268	0.420	96	36	1.3	6.26
61.850	1.4988	1.5026	0.120	222	36	2.9	0.90
62.795	1.4785	1.4822	0.180	64	35	0.8	1.14
63.490	1.4640	1.4677	0.180	69	35	0.9	2.80
64.015	1.4533	1.4569	0.120	114	35	1.5	1.64
65.245	1.4288	1.4324	0.150	56	34	0.7	1.07
65.860	1.4170	1.4205	0.300	37	34	0.5	1.66
67.715	1.3826	1.3860	0.120	279	32	3.7	3.58
68.140	1.3750	1.3784	0.090	357	32	4.7	1.12
68.280	1.3725	1.3759	0.090	400	32	5.3	1.21
68.880	1.3620	1.3654	0.120	196	32	2.6	1.37
69.475	1.3518	1.3552	0.240	137	32	1.8	3.31

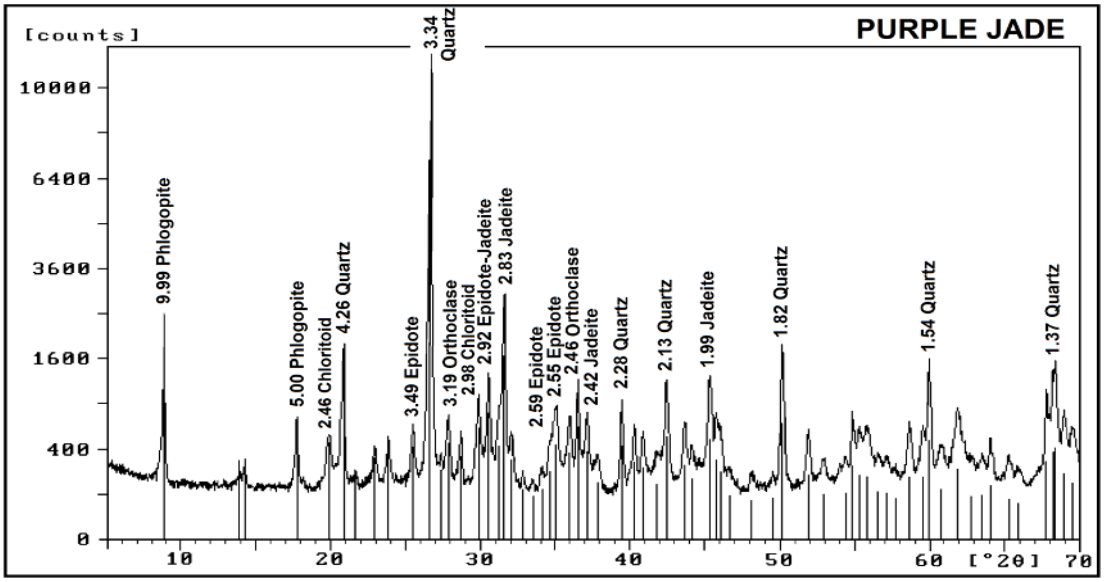

Figure 3.1 The XRD pattern of the representative Turkish purple jade sample, according to the numerical experimental XRD data in Table 3.1, showing the labels of the single or overlapped peaks of the base building mineral components of the purple jade bearing contact metamorphic aureole with a mineral assemblage consisting of mainly quartz, jadeite, orthoclase, epidote, chloritoid, and phlogopite in the Harmancık-Bursa region (Turkey). The positions of peaks with d-spacings [Å] and relative intensities [%(I/I_o)] are labelled for ≥ 4% of 2-theta values below 70 degrees.

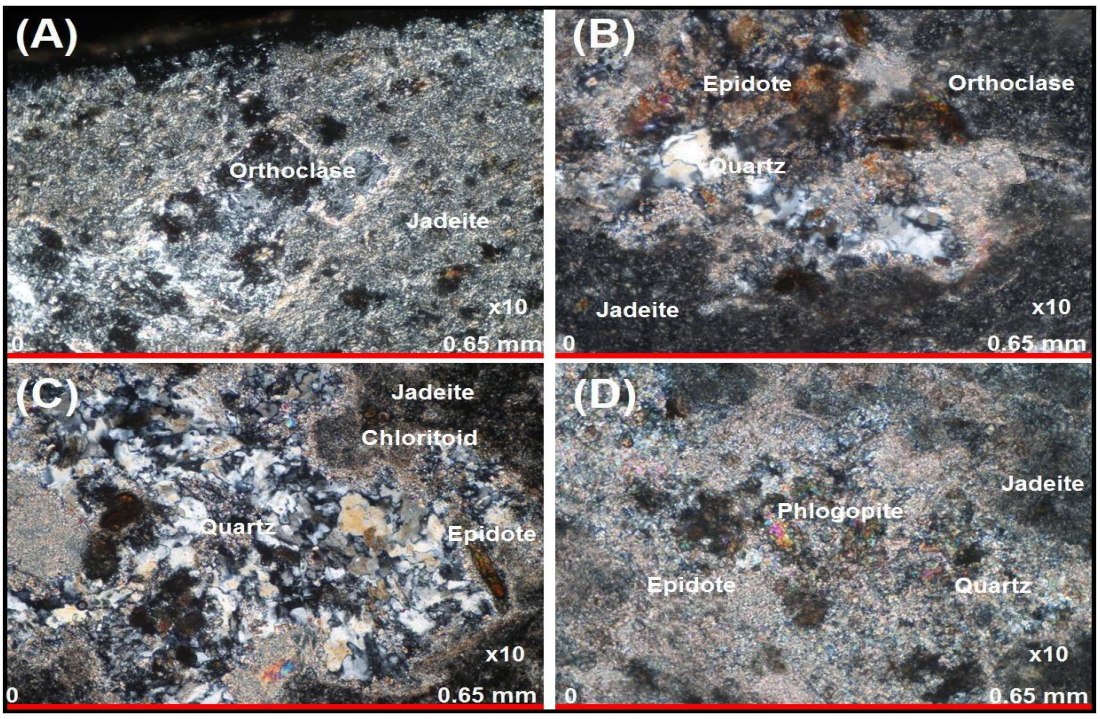

Figure 3.2 Microphotographs of the representative Turkish purple jade, viewed in crossed-polarized light (magnification, ×10). The main constituents are jadeite-orthoclase **(A)**, jadeite-quartz-epidote-orthoclase **(B)**, jadeite-quartz-epidote-chloritoid **(C)**, and jadeite-quartz-epidote-phlogopite **(D)**. It is seen that at least 40% of the volume of the extensive contact metamorphic aureole consists of observable jadeite crystallization with high relief and dark greenish-grey color; the volume of jadeite is over 60% in some places, In addition, there exist less important opaque minerals in the thin-sections. The width of the images is 0.65 mm.

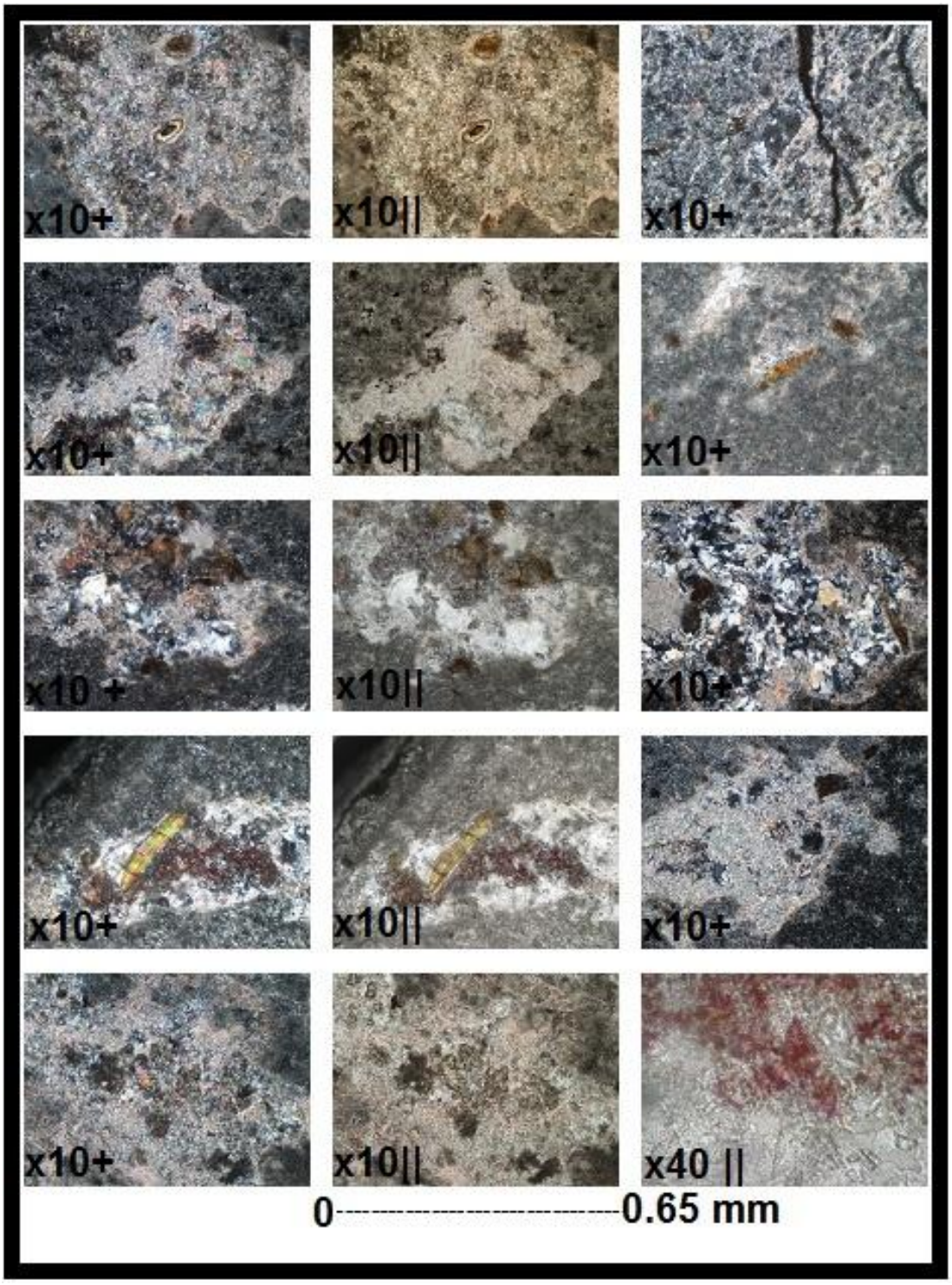

Figure 3.3 Various microphotographs of the representative Turkish purple jades. It is seen that at least 60% of the massive mass of the contact metamorphic aureole consists of readable jadeite crystallization with high relief and dark greenish-grey color. In addition, less important opaque minerals are present in the thin-sections.

Table 3.2 Average chemical bulk and trace element analyses of the Turkish purple jade samples from the Harmancık-Bursa region (Turkey). The significant concentrations of some main building elements, such as Al, Ca, Na, K, P, Sr, and Ba can be attributed to a calc-alkaline formation environment. In addition, significant concentrations of some trace elements, such as Fe, Cr, Mn, Be, Cu, Ga, La, Nb, Ni, Pb, and Zn are characteristics of the Turkish purple jade. Some of transition metal elements certainly are responsible for the production of both unique purple coloration and the characteristic Raman bands.

Oxides %	Instrument (XRF)	Sample	Elements	Instrument (ICP-AES)	Sample
	Detection limits	**Turkish purple jade**		Detection limits	**Turkish purple jade**
SiO_2	0.01 %	63.54			
Al_2O_3	0.01 %	20.17	Al	0.01 %	**8.52**
Fe_2O_3	0.01 %	1.78	Fe	0.01 %	**1.14**
CaO	0.01 %	2.70	Ca	0.01 %	**1.68**
MgO	0.01 %	0.35	Mg	0.01 %	0.18
Na_2O	0.01 %	6.71	Na	0.01 %	**4.55**
K_2O	0.01 %	1.74	K	0.01 %	**1.34**
Cr_2O_3	0.01 %	<0.01	Cr	1 ppm	**19**
TiO_2	0.01 %	<0.01	Ti	0.01 ppm	<0.01
MnO	0.01 %	0.22	Mn	5 ppm	**1540**
P_2O_5	0.001 %	0.048	P	10 ppm	**200**
SrO	0.01 %	0.03	Sr	1 ppm	**227**
BaO	0.01 %	<0.01	Ba	10 ppm	**80**
LOI	0.01 %	2.57			
Total	0.01 %	**99.86**			
			Ag	0.5 ppm	<0.5
			As	5 ppm	10
			Be	0.5 ppm	**4.7**
			Bi	2 ppm	<2
			Cd	0.5 ppm	<0.5
			Co	1 ppm	1
			Cu	1 ppm	**23**
			Ga	10 ppm	**40**
			La	10 ppm	**80**
			Mo	1 ppm	<1
			Nb	1 ppm	**72**
			Ni	1 ppm	**49**
			Pb	2 ppm	**15**
			S	0.01 ppm	<0.01
			Sb	5 ppm	<5
			Sc	1 ppm	1
			Th	20 ppm	20
			Tl	10 ppm	<10
			U	10 ppm	20
			V	1 ppm	3
			W	10 ppm	<10
			Zn	2 ppm	**95**

3.3 Specific Gravity Measurements

The hydrostatic balance (HB) method was used to analyse the Turkish purple jade samples with three different colorations. The values based on the formula ($SG = W_{air} / W_{air} - W_{water}$), were measured to be 3.05 in the intensely purple colored part, 3.02 in the pale purple and whitish mixed colored part, and 2.69 in the whitish and yellowish colored part (Figure 3.4). These results support the conclusions above since jadeite is the heaviest of the three major mineral components (SG = 3.24-3.42), quartz is lighter (SG = 2.65), and orthoclase also is heaveast (SG=2.53-2.56). The specific gravity values show that Turkish purple jade is a rock, a mixture of minerals, and not pure jadeite.

However, since the minor whitish and yellowish parts of the material are not used for gemstones, the average specific gravity value of the Turkish purple jade is 3.04.

In fact, this specific gravity value is unusual for jades composed of jadeite worldwide. Rather, the value is very similar to those of the jades composed of nephrite. In the literature, it has been proposed that the specific gravity range of the nephrite jades is 2.90-3.02. By contrast, well-known jadeite jades have a specific gravity range of 3.3-3.5 (Htein and Naing, 1994). The typical specific gravity of Turkish purple jade is thus distinctive—a bit too high for nephrite and much too low for jadeite. Therefore the hydrostatic balance method is a powerful tool to distinguish the Turkish purple jades from the other natural and synthetic jades.

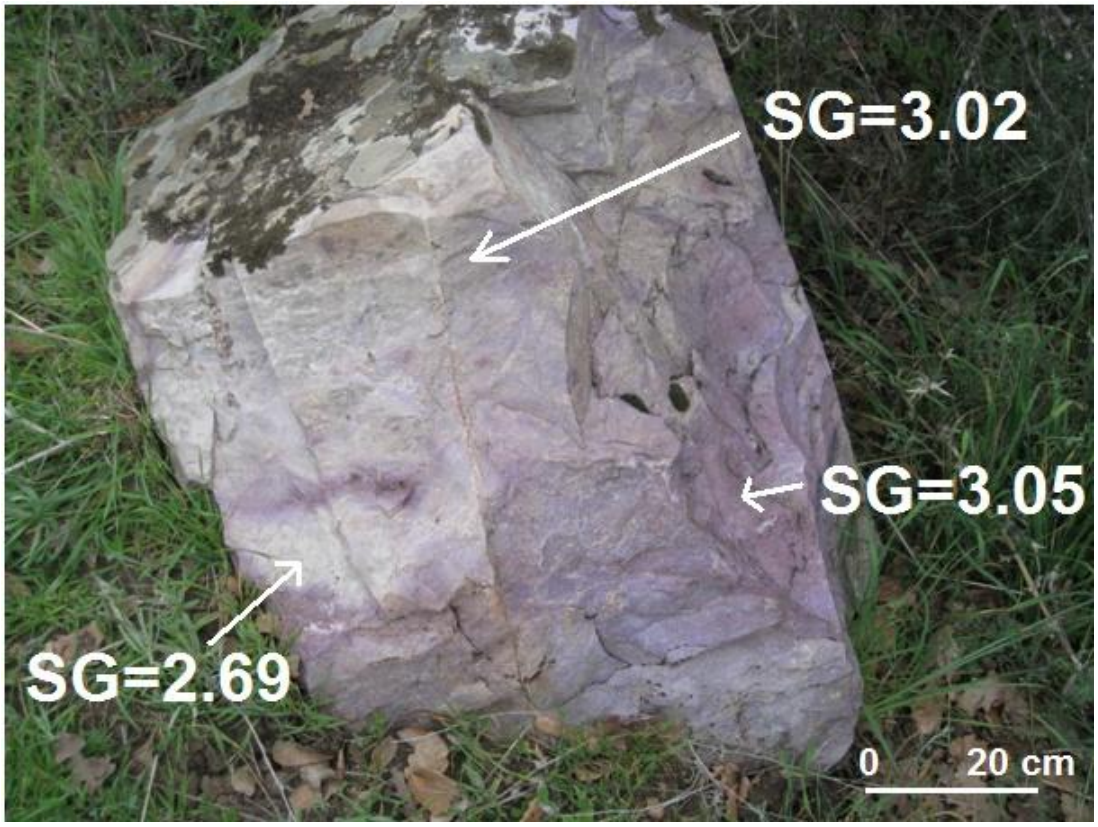

Figure 3.4 Specific gravity (SG) values of the Turkish purple jade material with three different colorations—this is a large block of the extensive contact metamorphic aureole. The values, based on the formula ($SG = W_{air} / W_{air} - W_{water}$), were measured to be 3.05 in the intensely purple colored part, 3.02 in the pale purple and whitish mixed colored part, and 2.69 in the whitish and yellowish colored part.

3.4 Chemical Constituents and Confocal Micro-Raman Vibrational Bands

Chemical analyses of the representative intensely purple colored Turkish jade samples were carried out using X-ray fluorescence (XRF) for major oxides and inductively coupled plasma-atomic emission microscopy (ICP-AES) for trace elements, and their chemical implications are given in order in Table 3.2.

Some rock building elements, such as Al, Ca, Na, K, P, Sr, and B of which characterize an acidic rock formation, and trace elements, such as Fe, Cr, Mn, Be, Cu, Ga, La, Ni, Pb, and Zn present remarkable high ratios**.** Hence, chemical impurities in the Turkish purple jade are present at significant concentrations for Fe (1.14%), Mn (1540 ppm), Be (4.7 ppm), Zn (95 ppm), Ni (49 ppm), Cu (23 ppm), Cr (19 ppm), and Pb (15 ppm) as transition metal elements, and for La (80 ppm) as a

rare earth element, and Ga (40 ppm) as a metalloid element (Table 3.2). Accordingly, we can interpret that pale purple coloration of this jade is owing to rich Mn^{3+} ions replacing a large number of Al^{3+} ions in the mass during the blueschist metamorphic facies formation in the region.

In addition, the result of the chemical bulk analysis indicates that the Turkish purple jade has significant concentrations of some main elements, such as Al, Ca, Na, and K as well as P, Sr, and Ba. In fact, these relatively higher ratios are important indicators for igneous rock formations of acidic-character. On the other hand, these relatively higher ratios mean that this unique material cannot be represented by a chemical formula like the ideally-known clinopyroxen composition [$Na(Al,Fe)Si_2O_6$], where chemical substitutions of Na (in the M2, Al (in the M1 site), or Si (in the tetrahedral site) are possible (Prewitt and Burnham, 1966; Htein and Naing, 1994; Zhao et al., 1994; Nestola et al., 2007).

The dispersive confocal micro-Raman spectra of the Turkish purple jade including vibration bands between 1600 and 50 cm^{-1} are given as the single spectrum including the bands characterized mainly jadeite (Figure 3.5), as the mapped multi spectra and related microscope images of them (Figure 3.6), and as the compared and contrasted combined spectra of them (Figure 3.7).

It is important that the micro-Raman vibrational bands of the Turkish purple jade have not been reported previously in the references related to jadeite-jade or nephrite-jade. Therefore, a total of characteristic 20 Raman bands of the Turkish purple jade were established even though some of them are closer values, and their causes were inferred (Table 3.3). These values have more peak numbers than those of other colored kinds of the jadeite-jades which have been reported by Zhao et al. (1994), Gendron and Smith (2002), Nestola et al. (2007), Bersani and Lottici (2008), and Fan et al. (2009), even though many of the peaks match exactly those of the Turkish purple jade.

As a result, the dispersive confocal micro-Raman bands centred at 1444, 1300, 1038, 984, 876, 776, 697, 571, 521, 464, 430, 372, 326, 307, 264, 218, 201, 143, 126, and 101 cm^{-1} are characteristics of the Turkish purple jade (Table 3.3). Moreover, the underlined ones are very strong bands.

In interpretation of the whole micro-Raman analysis for Turkish purple jade, it must take into account that at least 40% of the fine-grained material is jadeite (Figure 3.1), but significant amounts of quartz, orthoclase, chloritoid, phlogopite, epidote, and opaque minerals are also present (Figures 3.2 and 3.3 as well as 3.5).

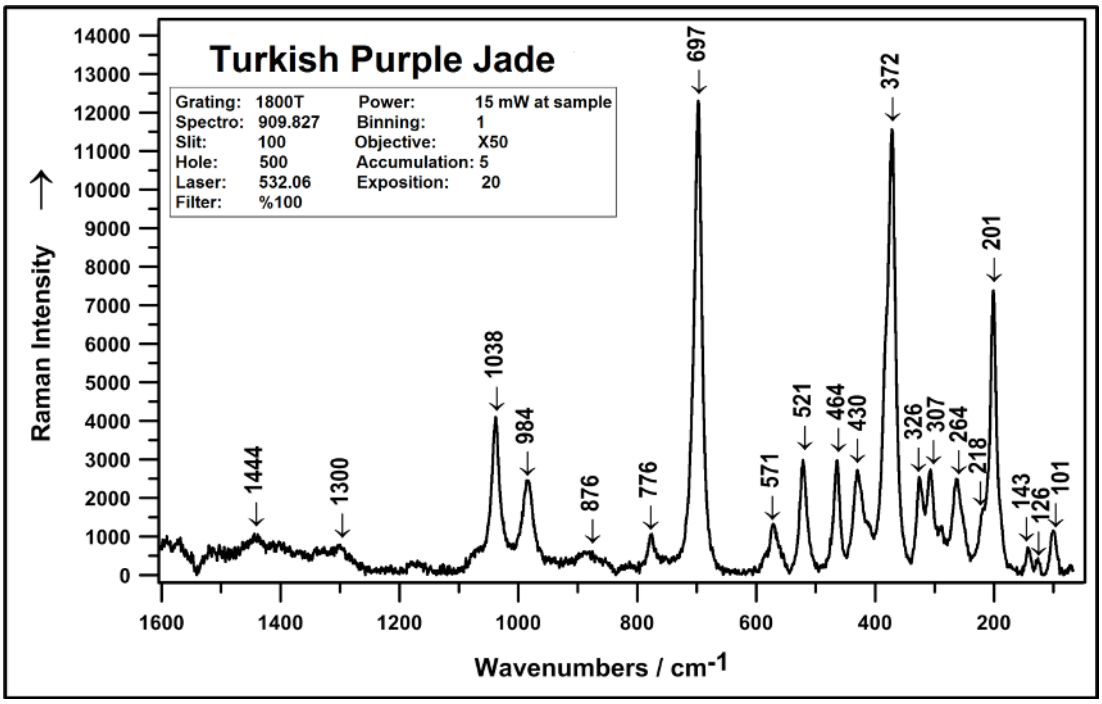

Figure 3.5 Micro-Raman vibrational bands of the Turkish purple jade to be a large portion of an extensive contact metamorphic aureole. The bands peaked at 1038, 697, 372, and 201 cm^{-1} represent the mineral jadeite (clinopyroxene subgroup) and are distinctive. The spectrum shows stretching and bending modes equivalent to those of polyhedral (mostly tetrahedral or octahedral) isolated molecules. The difference becomes clear by the cations generating *T* (translational) and *R* (rotational) libration modes.

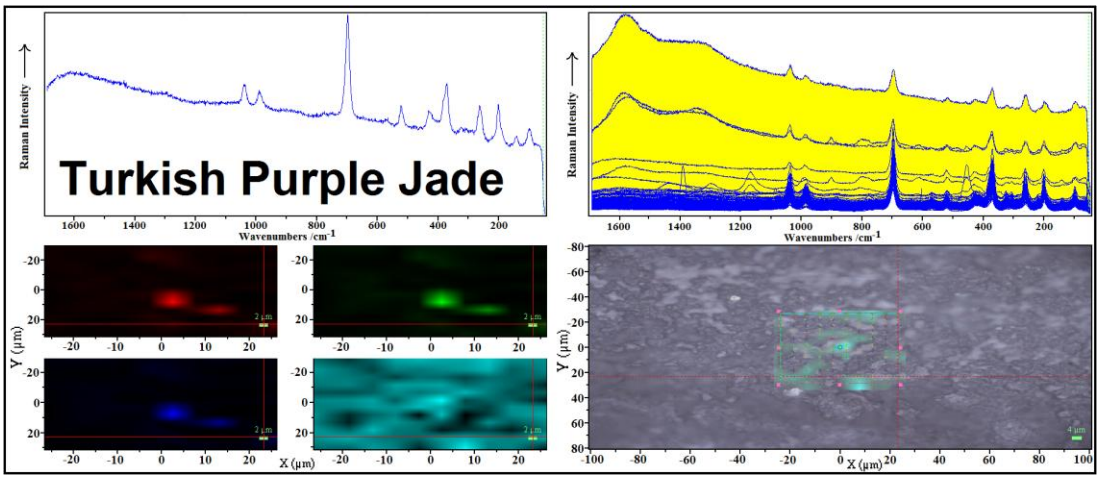

Figure 3.6 The mapped multi spectra and related microscope image of Figure 3.5. They show the variation of any fitted parameter (i.e. intensity, width or position of one band) as a function of the point of analysis. If the mapping is regular and sufficiently tight, one gets a ‘‘smart map’’ of the parameter (color or contrast scaling) superimposed with the optical image of the probed area.

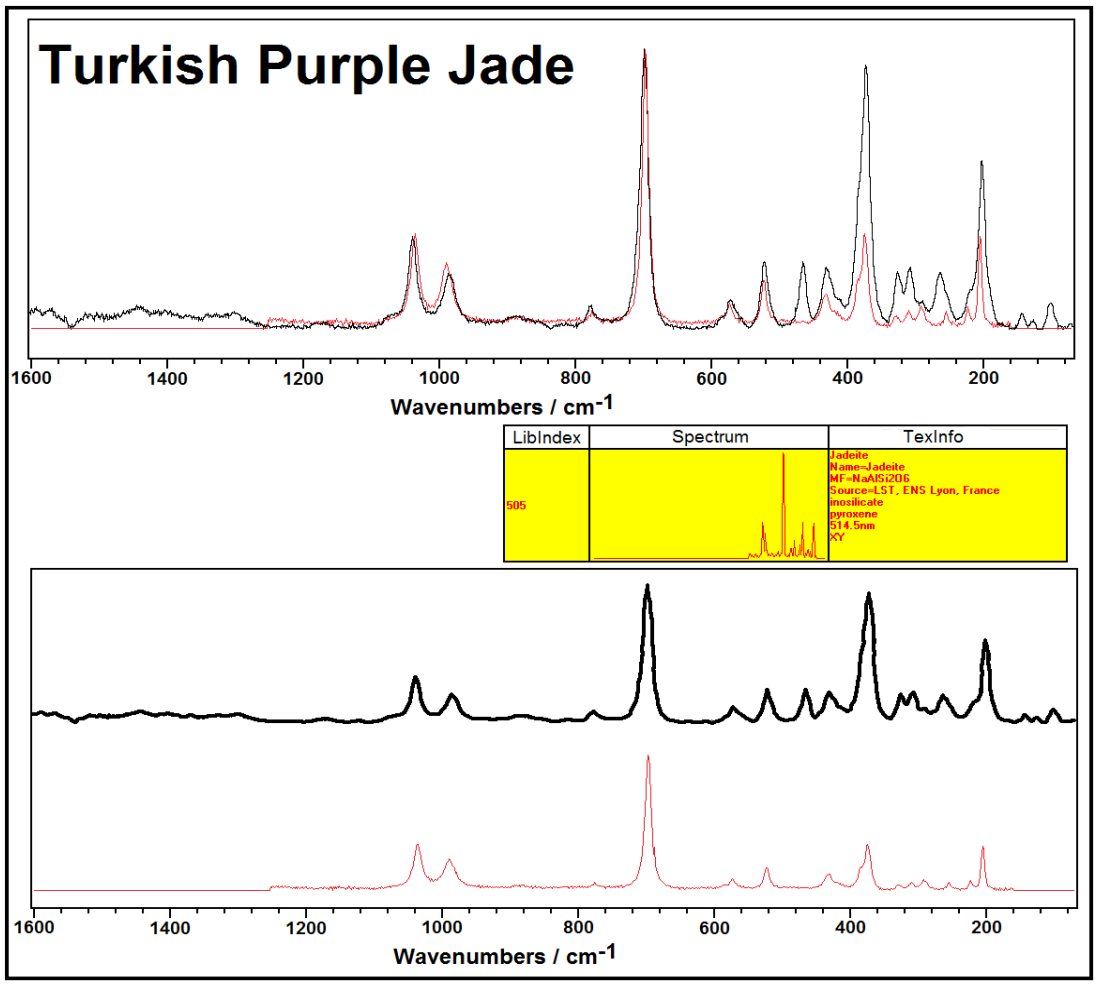

Figure 3.7 Comparison of the spectrum of the micro-Raman bands in Figure 3.5 for Turkish purple jade (black traces) with those of pure jadeite from anywhere (red traces).

Smith and Gendron (1997) has interpreted that the Si–O–Si symmetric stretching vibration of jadeite is affected by the nature of the M2 cation and, to a lesser extent, by the M1 cation: the wavenumber of the corresponding spectral band in the 650–750-cm^{-1} range may give indirect "chemical" information on the actual composition, after suitable calibration. As a result, the jadeite or nephrite nature of jade Chinese artifacts from the Trésor of the Muséum National d'Histoire Naturelle in Paris was determined by means of Raman spectroscopy: distinguishing features are the Si–O–Si stretching vibration at 675 cm^{-1} (nephrite) and above 695 cm^{-1} (jadeite), and are the presence of OH stretching vibrations for nephrite (Smith, 2005; Bersani and Lottice, 2010).

All collective vibrations in crystals can be viewed as the superposition of plane waves that virtually propagate to infinity. These plane waves (the normal modes of vibration) are commonly modelled by quasi-particles called photons. A normal coordinate of the form $Q= Q_0\cos(2\pi\nu n_{vib}t)$, which is actually a linear combination of bond lengths and bond angles, is associated with each normal mode. Depending on the dominant term in the normal coordinate, these modes can be classified as either stretching (n), bending (d), torsional (t), librational (R0/T0 pseudorotations / translations) or lattice modes (the latter include the relative displacement of the unit cells) (Gouadec and Colomban, 2007; Colomban, and Prinsloo, 2009; Slodczyk and Colomban, 2010; Vandenabeele, 2010).

These experimental data (Table 3.3) (Figures. 3.5, 3.6 and 3.7) of the Turkish purple jade indicate that the formation of distinctive vibrational bands is definitely related to lattice defects which can be attributed to some chemical impurities (external defects) and structural imperfections (internal defects) according to symmetry and main activity of SiO_4 tetrahedron with Td symmetry and C_{2v} symmetry in a D_{6h} structure (Colomban and Prinsloo, 2009).

The first most intensive and widest Raman band peaked at 697 cm^{-1} can be interpreted as being ν_2 doubly symmetric bending mode of [SiO_4/M] centres. The "M" includes the some cationic substitutions of Si by Fe, Cr, Mn, Be, Cu, Ni, Pb, and

Zn, and also K and Na. The second most intensive and widest Raman band peaked at 372 cm^{-1} can be interpreted as being ν_2 single symmetric bending mode of [SiO_4/M] centres. The third most intensive and widest Raman band peaked at 201 cm^{-1} can be interpreted as translational libration. Finally, the fourth distinctive Raman band peaked at 1038 and 984 cm^{-1} can be interpreted as being ν_1 doubly symmetric stretching modes of [SiO_4/M] centres.

Figure 3.6 shows that both sides of these bands were barricaded with some crystalline defect structures (imperfections) (Table 3.3).

According to dispersive confocal micro-Raman spectroscopy (DCμRS) in combination with quantitative analysis performed by ICP-AES, the productions of the Raman bands are mainly ascribed to the presence of relatively higher concentrations of some transition metal elements, such as Fe, Cr, Mn, Be, Cu, Ni, Pb, and Zn in [SiO_4/M] centres, which can be attributed to extrinsic defects (chemical impurities) derived from the intrusive granodiorite that gave rise to the contact metamorphic aureole in the region. Since, it is well-known that elements with high atomic numbers that are situated on the right side of the periodic table (covalent materials in general) are good Raman scatters whereas ionic structures are difficult to analyse with Raman spectroscopy. Some transition metal ions from the 3*d* (chromium) or 4*f* (lanthanides) groups produce strong fluorescence signals which often mask the Raman spectra but can be used for short range structure and/or residual stress assessment (Delé-Dubois et al., 1986; Gouadec and Colomban, 2007; Colomban, and Prinsloo, 2009; Vandenabeele, 2010).

Meanwhile, these elements are caused by the presence of relatively higher concentrations of some main building elements, such as Na and K in [AlO_4/M^+] and [SiO_4/M^+] centres, which can be attributed to extrinsic defects (chemical impurities), and additionally, to intrinsic defects (the nonbridging oxygen deficient centres with several precursors, self-trapped exciton, and dislocations) to being resulted from the long and strong metamorphism conditions during the Tertiary.

Gouadec and Colomban (2007) have stated that the width of the other Raman modes is mainly sensitive to the ‘‘local’’ crystal field, more specifically to the short range order in the first (0.1-0.5 nm) and second (0.5-5 nm) atomic shells. If the ‘‘molecular’’ description of vibrations applies, then Raman bending modes are even specifically sensitive to local geometric disorientation and Raman stretching modes to the neighbouring disorder (particularly atoms from other sub-lattices or electric defects to be resulted from substitutions /vacancies).

Some main building elements of the Turkish purple jade indicate that the bands in the spectra can be mainly attributed to extrinsic defects (chemical impurities) which are due to increasing amounts of tetrahedral character with increasing electron density caused by the presence of trace elements, taking into consideration the increased ionic character of the Si-O bonds in the alkali silicate, and can be partially attributed to intrinsic defects (the nonbridging oxygen deficient centres with several precursors and self-trapped exciton). Nutall and Weil (1980) reported a hydrogenic trapped hole-centre with four hydrogen atoms in a regular silicon lattice position. Since, in the case of some elements, compensation of the electric charge is necessary, additional cations such as H, Li, Na., K, and Ag can be incorporated in inter-lattice positions in conjunction with structural channels. However, the contribution of ionic bonds like Al-O is null according to that of covalent Si-O bonds (Colomban, and Prinsloo, 2009). So, the considerable strength of the Si–O bond results in a high melting temperature (Colomban, and Prinsloo, 2009). The basic unit of a silicate, the SiO_4 tetrahedron, is a strong chemical entity and the possibility to share oxygen atoms between two tetrahedra with variable Si–O–Si angles or to have non-bridging oxygen atoms gives a polymeric character to silicates (Colomban, and Prinsloo, 2009). The $[SiO_4]^o$ centre is caused by substitution for Si^{4+} with an electron hole at one of the four nearest O^{2-} ions, forming O^- .The nonbridging oxygen hole centre (≡Si-O) is described as a hole trapped in a single oxygen atom bound to a single silicon on three oxygen atoms in the SiO_2 structure (Weil, 1984). Oxygen excess centres include the peroxy radical (≡Si-O-O), an oxygen associated hole centres consisting of an O^{2-} ion bonded to single silicon on three oxygen atoms, and the peroxy linkage (≡Si-O-O≡). Because of the negative net charge, additional trivalent

substitutes of the Si^{4+} positions occur as charge compensation (i.e. Al^{3+}) in such a way that an additional proton is bound on the Al^{3+} (Colomban, and Prinsloo, 2009; Vandenabeele, 2010).

Slodczyk and Colomban (2010) have stated that many electrical/electrochemical/magnetic properties result from a competition between different potentials of the chemical bonding and structure. In general, some atoms (alkali and earth alkali cations) have a strong ionic character. Some other atoms develop covalent bonding (i.e., transition metals) and form strong "molecular" bricks. Metallic bonds can also be formed between atoms such as Ag, Cu, Tl, and can be ionized clusters intermediately between ions and complex nano-clusters may be observed.

In granitic rocks, green- and white-colored jadeite-jade occurrences are rare (Bersani and Lottici, 2008); however, purple-colored jade occurrence is the rarest. Hence, granites and similar host rocks have been intensely reworked by post-magmatic and host-rock fluids, resulting in intense re-crystallisation, enrichment in Na, Al, Fe and rare elements, and replacement of primary muscovite and sodic-calcic clinopyroxens (i.e.. diopside) in order to produce typical single-jadeite crystallization [$Na(Al,Fe)Si_2O_6$] (Rossi et al., 1983; Brizi and Mellini, 1992; Nestola et al., 2007).

In addition, micro-Raman spectroscopy has been used to investigate bleached and filled jadeite jade: bleaching with strong acid produces micro-cracks, which are filled with epoxy resin, evidenced by the Raman shifts close to 777, 1123, 1611, 2930, and 3065 cm^{-1}. Moreover, it is possible to identify bleached jade by distinguishing resin from paraffin (Fan et al., 2007 and 2009; Bersani and Lottici, 2010). In particular, Fan and his colleagues (2007 and 2009) have pointed to a research conducted using a NIR Raman spectrometer for a large number of jadeite samples, and they have reported that NIR (785 nm) Raman spectrometer exhibits advantage of non-destruction, quickness, accurateness, and weak fluorescence interferences.

On the other hand, the results of the chemical trace element analysis, which shows some transition metal elements such as Fe, Cr, Mn, Be, Cu, Nb, Ni, Pb, and Zn, metalloid element such as Ga, and rare-earth element such as La, indicate that higher presence of constitutive trace elements is one of the most important characteristics of the Turkish purple jade. Some of these are certainly responsible, as external lattice defects, for producing the unique purple color. The colors of all kinds of jadeite-jades are due to the presence of impurity elements, as reported in previous papers (Harder, 1995). For example, the presence of iron and/or chromium imparts a green color to the mineral (Rossman, 1974). Manganese provides a lavender color (Nassau and Shigley, 1987; Fan et al., 2007 and 2009). However, the unique purple coloration of the Turkish jade is due to a more complex mechanism, since many transition metal coloration agents are present in it. In order to clarify the purple color formation, further investigation will be necessary.

Table 3.3 Confocal micro-Raman vibrational bands of the unoriented sample of the representative Turkish purple jade from the Harmancık-Bursa region (Turkey), and their inferred causes according to symmetry and main activity of SiO_4 tetrahedron.

Peak Number	Micro-Raman Bands Wavenumbers / cm^{-1}	Inferred Causes
1	**1444**	Nonbridging oxygen hole centres with several precursors (i.e., peroxy linkage) and oxygen vacancy.
2	**1300**	Nonbridging oxygen hole centres with several precursors (i.e., peroxy linkage) and oxygen vacancy.
3	**1038**	ν_1 doubly symmetric stretching modes of [SiO_4/M] centres.
4	**984**	
5	**876**	ν_1 doubly symmetric stretching modes of degeneracy of [SiO_4/M] centres.
6	**776**	
7	**697**	ν_2 doubly symmetric bending mode of [SiO_4/M] centres. The "M" includes the some cationic substitutions of Si by Fe, Cr, Mn, Be, Cu, Ni, Pb, and Zn, and also K and Na.
8	**571**	ν_2 fourthly symmetric bending modes of degeneracy of [SiO_4/M] centres.
9	**521**	
10	**464**	
11	**430**	
12	**372**	ν_2 single symmetric bending mode of [SiO_4/M] centres.
13	**326**	Rotational libration mode.
14	**307**	Rotational libration mode.
15	**264**	Rotational libration mode.
16	**218**	Rotational libration mode.
17	**201**	Translational libration.
18	**143**	Translational libration mode.
19	**126**	Translational libration mode.
20	**101**	Translational libration mode.

3.5 Luminescence Features

It is well-known that luminescence is the emission of light from a mineral when excited by

- UV (photoluminescence, PL)
- X-rays (radioluminescence, RL)
- Electrons (cathodoluminescence, CL)
- Heat (thermoluminescence, TL).

During this investigation, four different luminescence spectra of the Turkish purple jade samples [photoluminescence (PL), radioluminescence (RL), cathodoluminescence (CL), and thermoluminescence (TL)] were taken into consideration, and evaluated (Figures. 3.8-3.13).

Indeed, perfect-structured crystalline materials emit very little light when excited by irradiation and/or heating. Therefore, all kinds of luminescence of the minerals (and materials) tell us about the crystalline defects that occur in all natural solids. These are (1) chemical impurities, such as trace elements, (2) structural imperfections, such as vacancies (holes where atoms should be), elements with the wrong charge (O^{1-} where O^{2-}should be), dislocations (where bonds do not join up properly), and (3) many others (Blasse and Grabmaier, 1994; Gaft, 2005; Handerson and Imbusch, 2006).

3.5.1 Photoluminescence (PL)

Photoluminescence (PL) excitation emission scans of the Turkish purple jade are first time obtained as three-dimension (3-D) to characterize a variety of the material parameters, and given in Figures 3.8 and 3.9. These spectral characteristics obtained by photoluminescence (PL-3D) excitation emission scans ranging between 300 and 900 nm of wavelengths, and between 220 and 340 K of temperatures, are unique to the Turkish purple jade. Accordingly, a total of 6 maxima peaks in the visible region (400-700 nm) appear about at 743, 717, 698, 484, 465, and 442 nm, respectively. It is seen that two wider major bands are observable on the spectrum. The first one

appears at the low temperatures and in the orange-yellow region only. Its maxima peaks are seen mainly about at 743, 717, and 698 nm. This first wide band damps through the higher temperatures. The second one appears at the low temperatures, and continues until to the higher temperatures. This second relatively wider band covers the blue and violet regions, and its maxima peaks are seen mainly about 484, 465, and 442 nm.

In fact, what cause photoluminescence (PL) as well as the other luminescence are lattice defects as either chemical impurities or structural imperfections (Blasse and Grabmaier, 1994; Gfroerer, 2000; Gaft et al., 2005; Handerson and Imbusch, 2006). Therefore, individual PL bands appeared at the end of the excitation emission scans can be attributed to some defects related to heterogeneous structure in the Turkish purple jade samples with a mineral assemblage consisting of mainly jadeite, quartz, orthoclase, epidote, chloritoid, and phlogopite minerals. However, in an EPR study performed on the single jadeite mineral samples, it has been stated that the signals, which increase with absorbed dose, were because of electron centres (Teixeira et al., 2010). Thus, we can claim that the majority of these defects related to heterogeneous structure come from the cationic substations. Since, PL spectroscopy provides electrical (as opposed to mechanical) characterization, and it is a selective and extremely sensitive probe of discrete electronic states (Gfroerer, 2000). On the other hand, in the case of obtaining information on the quality of surfaces and interfaces in the heterogeneous structured purple jades, it is revealed that the intensity of the PL signals readable increase in the regions of orange-yellow, blue, and violet instead of the regions red, green, and purple. So, we can also claim that the structural imperfections of the electron centres which produce the strong PL-3D morphology (Figures. 3.8 and 3.9) become more effective in the interval color (orange-yellow-blue-violet) regions than the base color (red-green-purple) regions.

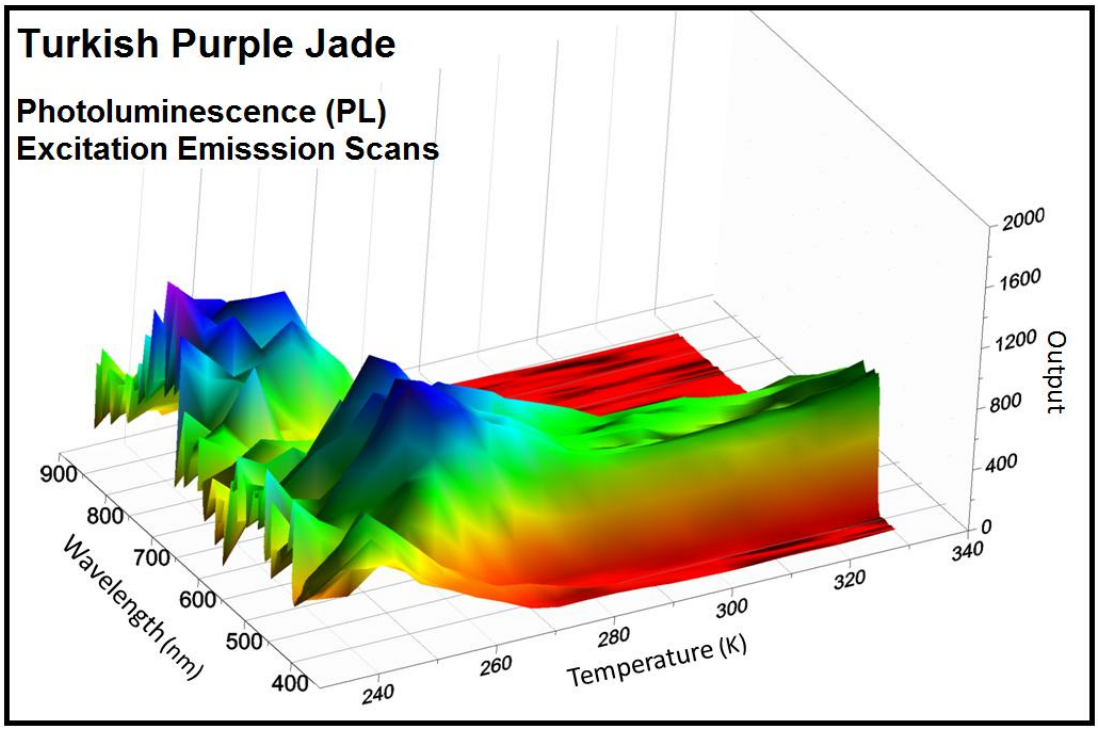

Figure 3.8 Photoluminescence (PL-3D) morphology of the heterogeneous-structured Turkish purple jade. Maxima peaks in the visible region (400-700 nm) are measured about at 743, 717, 698, 484, 465, and 442 nm respectively.

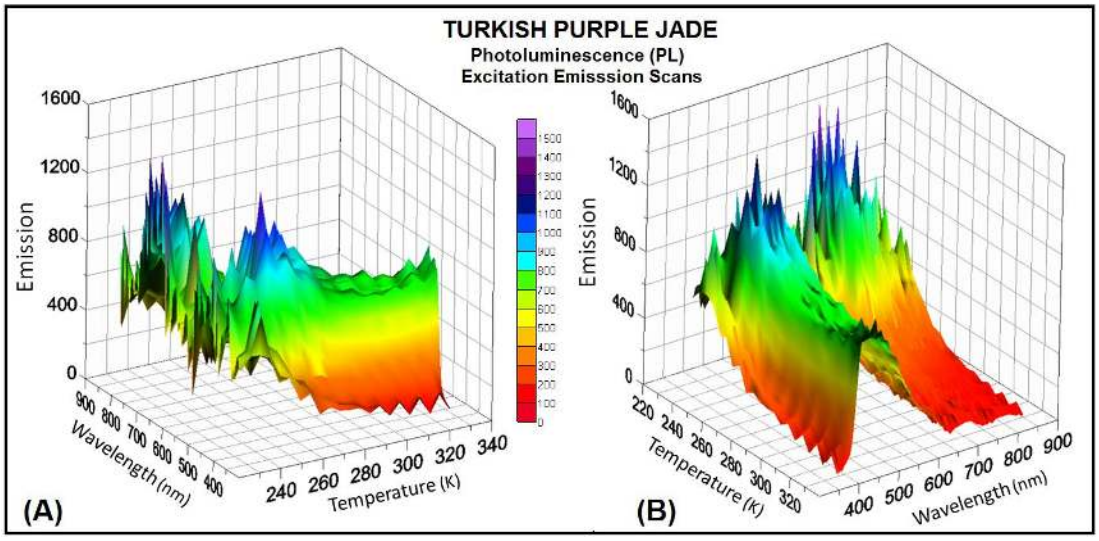

Figure 3.9 Two different profile views [from the front-side (A) and the back-side (B)] of photoluminescence (PL-3D) excitation emission scans of the purple jade.

3.5.2 Radioluminescence (RL)

Radioluminescence (RL) spectrum of the Turkish purple jade was presented as three-dimension (3-D), and given in Figure 3.10. We thought that the RL spectrum

obtained as X-ray induced luminescence against to heating is a sensitive technique for studying defects in the heterogeneous-structured purple jade material. During this analysis, X-radiation was penetrated and then excited the whole volume of the jade material, forming new luminescence defects (Gaft et al., 2005). Moreover, one of the most suitable methods is that RL light is detected by high-sensitivity wavelength multiplexed TL system (Luff and Townsend, 1993). It is well-known that RL generates electrons and holes as well as filling trapping sites, whereas the TL only generates recombination of charges, which were previously trapped. Although there was not intense emission in the region of interest, experiments revealed some interesting results. A radioluminescence band peaked at around 550 nm is very important and individual, since it decreases with temperature and is undetectable beyond 185 K. It does not represent a conventional glow curve such that it decays gradually during the heating, but suddenly disappears beyond 185 K. These results may tentatively be interpreted by a process of energy transfer between jade material lattice and impurity ions. In addition, individual long-wavelength luminescence peaked at about 820 nm starting at 150 K has been observed. As it is well known, Cr^{3+} exhibits an emission line at approximately 650 nm at room temperature which must be assigned to an impurity emission. Time-resolved studies as well as the excitation spectra show that the impurity emissions result from energy transfer from the jade material lattice (exciton capture) rather than from direct absorption. The impurity emission is assigned to the electron transitions of the Cr^{3+} ion from lower (^3E) to higher (^5E) energy levels (Tuncer-Arslanlar et al., 2011). In addition, there is evidence for a weak emission peaked at about 820 nm of the near infrared region, which appears to arise from the ^3E to $^3T1$ transition of the Cr^{3+} ion (Vanoy et al., 1988). At low temperatures the ^3E state lifetimes range between 150 mμs and 1.1 mμs depending on the jade material lattice. Emission from the ^3E state is an unexpected observation since the ^3E state is not the lowest energy excited state of the Cr^{2+} ion (Tuncer-Arslanlar et al., 2011).

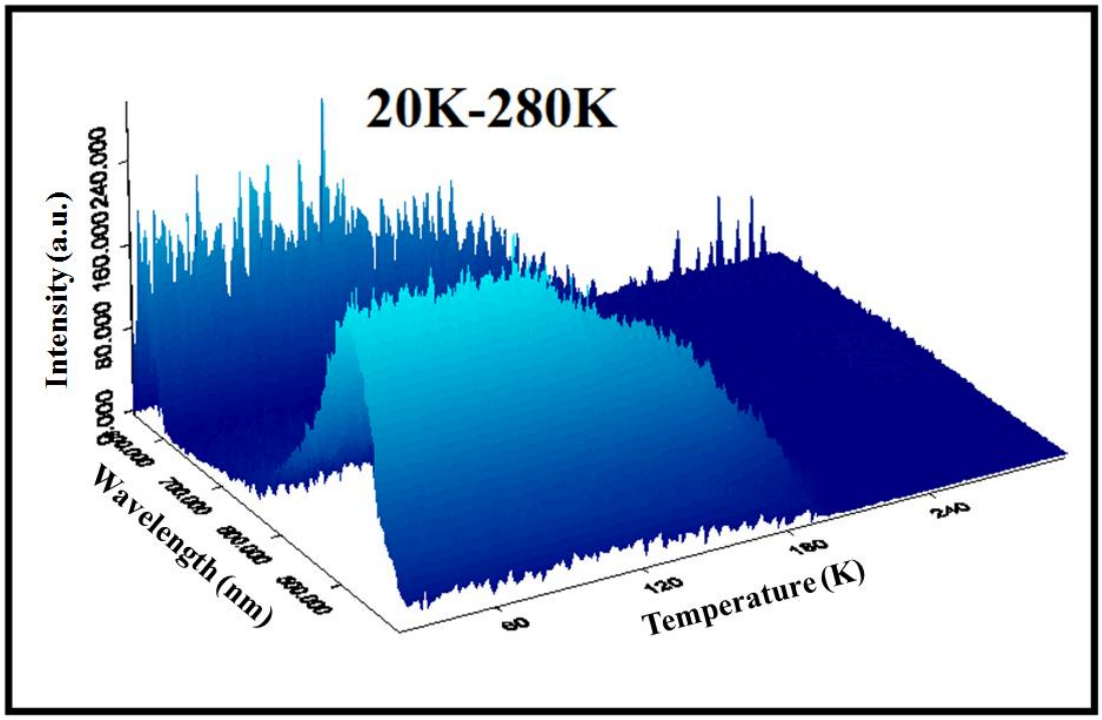

Figure 3.10 The radioluminescence (RL-3D) morphology of the Turkish purple jade. Maxima peaks in the visible and near infrared regions (400-900 nm) are measured about at 550, 650, and 850 nm, respectively [modified and inferred from Tuncer-Arslanlar et al. (2011)].

3.5.3 Cathodoluminescence (CL)

Cathodoluminescence (CL) results at room temperature obtained using measurements with alternating current (AC) at 14 kV energy (temperatures of 300 and 77 K) are given in Figures 3.11 and 3.12. Accordingly, a relation can be observed between the CL emissions and presence of some transition metal elements. Changes in the relative intensities of the CL bands can be observed when different excitation modulation frequencies are used. However, it is obvious that all trace elements do not play a direct role.

Gaussian fitting of the cathodoluminescence AC experimental data at 14 keV energy and 300 K temperature, and at the frequencies of 90, 180, 360, and 900 Hz indicates that two major spectral emission bands appear in readable intensity and magnitude at 90 Hz in the middle-visible wavelength region (yellow region) at about 610 nm, and in the longer-visible wavelength region (orange-red region) at about 670

nm (Figure 3.11). However, the intensities of the spectral emission bands at the other frequencies are very low, and thus they can be neglected. On the other hand, Gaussian fitting of the cathodoluminescence AC experimental data at 14 keV energy and 77 K temperature, and at the frequencies of 9, 90, and 180 Hz indicates a major spectral emission band that appears in readable intensity and magnitude at 9 Hz in the shorter-visible wavelength-visible (blue region) at about 470 nm (Fig 3.12).

It is seen that all peaks decrease sharply as the excitation modulation frequency increase. The fact that such changes are apparent at the very low frequencies of modulation immediately indicates that there are some very long lifetime processes occurring. Obviously, these initial spectral emissions shift from the orange-red and yellow regions to the blue region. This shift in the low temperature can show an electrical charge changing reaction in the polycrystalline jade structure with developing a strained Al(Si)–O–Mn and Al(Si)-O-Fe bonds. In the previously published paper, Götze and his colleagues have stated that the most significant activators of CL in feldspars and some pyroxenes are Al^{3+} and trace elements including Mn^{+2}, Ti^{3+}, Fe^{+2}, Fe^{+3}, Cr^{+3}, Pb^{+2}, Eu^{3+} as well as some rare earth elements (REE) (Götze, 2000; Götze et al., 2000). On the other hand, Tuncer-Arslanlar and her colleagues (2011) have drawn attention to the luminescence activators of the Turkish jade in their recent study. Accordingly, they point to the strong dependence of the peak-wavelengths and intensities of CL on the spatially varying concentrations of Na and K (as well as more random changes in other trace impurities), because of observing under the chemical EDS Na-jadeite and some patches or areas of K-Jadeite with a little more potassium than sodium. Therefore, when they recorded data in order to see influences on CL spectrum of both Na-jadeite and K-jadeite, it was seen that the most striking features of the analyses where CL was compared between Na-jadeite and K-jadeite for spectral bands of 326 nm (UV) and 565 nm (green).

The observed effects can be explained by known relations that the peak position of the red luminescence emission in feldspars can be affected both by the structural state of the feldspar and the site occupancy of the trivalent iron (Krbetschek et al., 2002; Garcia-Guinea et al., 2007).

As a result, we can suggest that remarkable luminescence emission in the Turkish purple jade is probably due to the silicon-oxygen and aluminium-oxygen stresses. These strained structures with Si–O bonds stabilise some non-bridging oxygen or silicon vacancy hole centres or some of the Si–O bonding defects which seem to be finally responsible for this UV emission. Accordingly, representative jade samples exhibit a pale purple color related to Mn^{2+} and Fe^{3+} color centres. These ions also contribute to a strong CL luminescence at about 610 and 770 nm. In a hydrogen atmosphere, charoite turns white and a more intense 600 nm luminescence peak is enhanced by reductive reaction Mn^{2+} to Mn^{3+}. Since, Mn^{2+} is the most important activator element. Variations in the amount of structurally incorporated Mn^{2+} cause variations in the intensity of the yellow emission band at about 610 nm.

In a recent study, the origin of blue band in the various jades was connected to the presence of one or more unknown defect centres (Ponahlo, 1999). However, the CL analyses of tectosilicates concluded that peaks in the 400 nm-range are correlated with the abundance of Al^{3+} or Eu^{2+}. Table 2 shows that the influence of Al^{3+} on the intensity of this peak is significant. When it is well-correlated with the presence of Ti^{2+} and Ca^{2+}, several other peaks may be hidden under the envelope of broad bands. Therefore rather than viewing just the original wavelength signals, the data should be transformed into energy plots (i.e. these transform both the wavelength axis into photon energy, and the ordinate from signals based on the fixed bandwidth of the spectrometer, $I(\lambda)d\lambda$ to the energy version of $I(E)dE$). Such transformations can greatly alter ones perspective of which is the dominant emission features.

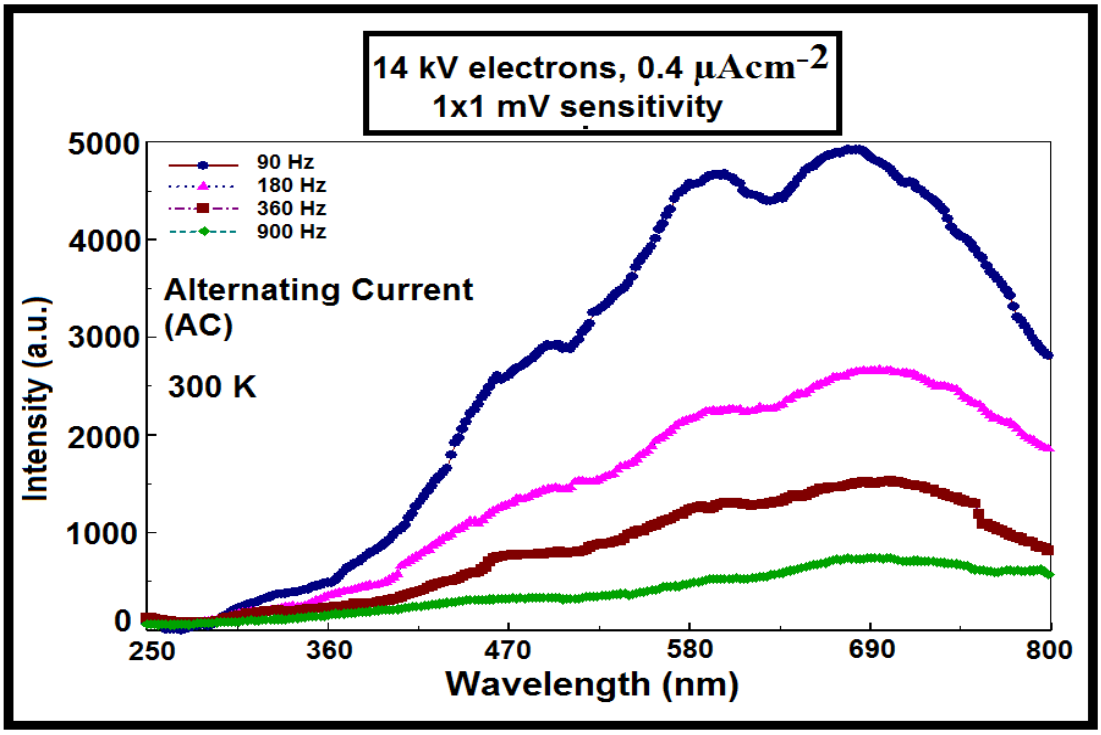

Figure 3.11 Cathodoluminescence (CL) spectra at 300 K of the Turkish purple jade. Two major spectral emission bands appear in readable intensity and magnitude at 90 Hz in the middle-visible wavelength region (yellow region) at about 610 nm, and in the longer-visible wavelength region (orange-red region) at about 670 nm [modified and inferred from Tuncer-Arslanlar et al. (2011)].

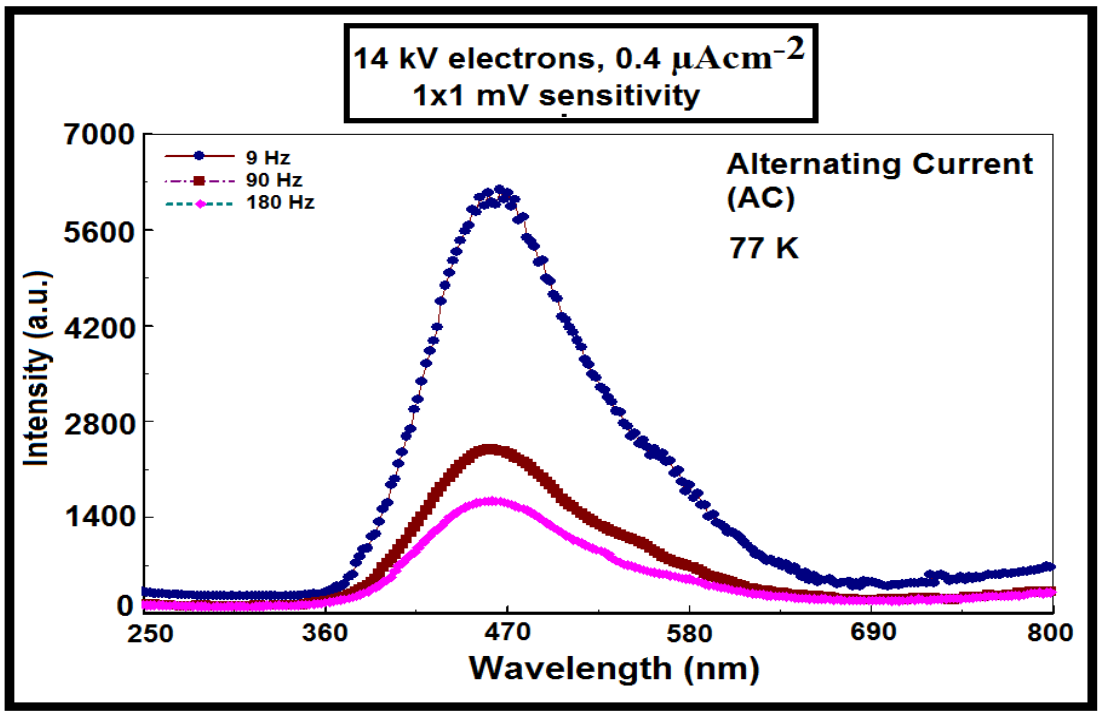

Figure 3.12 Cathodoluminescence (CL) spectra at 77 K of the Turkish purple jade. A major spectral emission band appears in readable intensity and magnitude at 9 Hz in the shorter-visible wavelength-visible (blue region) at about 470 nm [modified and inferred from Tuncer-Arslanlar et al. (2011)].

3.5.4 Thermoluminescence (TL)

The thermoluminescence glow curves obtained as a result of a linear heating rate of 2 Cs^{-1} in N_2 atmosphere at 300 K, have a great importance for characterizing the extent of utility of the Turkish purple jade to be used in measuring the radiation doses (Figure 3.13).

Accordingly, it is seen that main glow curves on the pattern appears as the widest and highest bands peaked at nearly 95 ^{o}C at the end of the heating of 10 minutes, and at nearly 110 ^{o}C at the end of the heating of 30 minutes. We can state that the glow curve of the purple colored jade from Turkey is highly different from the green and/or whitish colored jades from the other worldwide countries, which they have been reported by Melo et al (2004). This difference can be attributed to the formation conditions of the contact metamorphic aureole in the Harmancık-Bursa region. In this regard, we can claim that a thermolominescence glow curve of the Turkish purple jade is one of the characteristic provenance identification methods.

The dosimetric properties of lavender jadeite similar to these materials have already been studied using the thermoluminescence technique, showing their potential use for high-dose dosimetry (Melo et al., 2004).

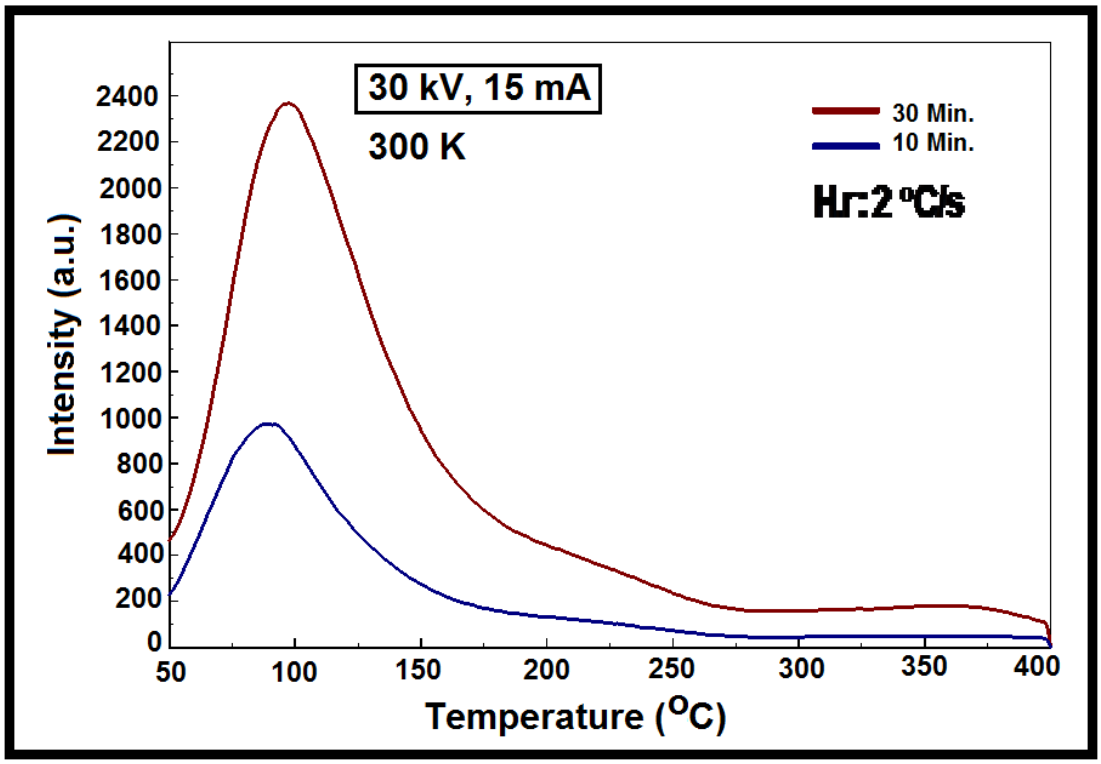

Figure 3.13 Thermoluminescence (TL) glow curves of the Turkish purple jade sample. Main glow curves on the pattern appears as the widest and highest bands peaked at nearly 95 °C at the end of the heating of 10 minutes, and at nearly 110 °C at the end of the heating of 30 minutes [modified and inferred from Tuncer-Arslanlar et al. (2011)].

CHAPTER FOUR
CONCLUSIONS

From the region comprising the Harmancık-Bursa region in Turkey, some tons of the purple-colored jade material that occur a metamorphic zone at the border between a coherent blueschist metamorphic sequence and an intrusive granodiorite have been illegally exploited, and exported as specifically named "Turkish (and/or Anatolian purple jade" since the 1980s.

This study focuses on purple jade identification and on the evaluation of the composition, provenance, and genesis of this kind of jade gemstone.

Turkish purple jade samples are found as massive-structured fine-crystalline masses. Therefore, they have an opaque appearance and generally a pale purple color. When the main mineral contents of a contact metamorphic aureole mass are identified by the convensional petrographic technique under a polarizing microscope as destructive and by the dispersive confocal micro-Raman spectroscopy as non-destructive, it is seen that main constitutive components of this contact metamorphic aureole mass are identified as non-destructive using confocal micro-Raman spectroscopy.

An application of dispersive (visible) confocal micro-Raman spectroscopy (DCμRS) was carried out to reveal a natural metamorphic zone for the characterization and provenance. A confocal micro-Raman spectrometer and hydrostatic balance are the most accurate non-destructive and non-invasive tools to distinguish the natural purple jades from other colored natural and synthetic jades and to identify their provenance regarding geographic region. Thus, it can be proposed that confocal micro-Raman spectroscopy could play a much more important role in the gemmology field.

The dispersive confocal micro-Raman spectroscopy (DCμRS) was performed on the Turkish purple jade, and possible causes of the vibrational bands were attributed

to some crystalline defects (impurities and imperfections) with reference to the ICP-AES analysis. Some rock building elements, such as Al, Ca, Na, K, P, Sr, and B, and trace elements, such as Fe, Cr, Mn, Be, Cu, Ga, La, Ni, Pb, and Zn were found in the remarkable high ratios**.** These vibration bands can be mainly attributed to extrinsic defects (chemical impurities) due to increasing amounts of tetrahedral character with rising electron density caused by the presence of trace elements, taking into consideration the increased ionic character of the Si-O bonds in the alkali silicate, and can be partially attributed to intrinsic defects (the nonbridging oxygen-deficient centres with several precursors and self-trapped exciton). They are mainly ascribed to the presence of relatively higher concentrations of some transition metal elements, such as Fe, Cr, Mn, Be, Cu, Nb, Ni, Pb, and Zn in [SiO_4/M] centres which can be attributed to extrinsic defects (chemical impurities) derived from the contact metamorphic aureole stock in the region. At the same time, we can interpret that pale purple coloration of this jade is due to the rich Mn^{3+} ions replacing a large number of Al^{3+} ions in the mass during the blueschist metamorphic facies formation in the region.

The rapid mapping capabilities allow for large scale survey maps to be collected with smaller higher spatial resolution maps obtained once a region(s) of interest has been located. This technology has been used to investigate the Turkish purple jade.

Two wider major photoluminescence (PL) bands are observed. The first one appears at the low temperatures and in the orange-yellow region only. Its maxima peaks are seen mainly about at 743, 717, and 698 nm. This first wide band damps through the higher temperatures. The second one appears at the low temperatures, and continues until to the higher temperatures. This second relatively wider band covers the blue and violet regions, and its maxima peaks are seen mainly about 484, 465, and 442 nm. It can be stated that the structural imperfections of the electron centres which produce the strong PL-3D morphology become more effective in the interval color (orange-yellow-blue-violet) regions than the base color (red-green-purple) regions.

Three remarkable radioluminescence (RL) bands are observed. Maxima peaks in the visible and near infrared regions (400-900 nm) are measured about at 550, 650, and 850 nm respectively.

Cathodoluminescence (CL) results display original patterns. Two major spectral emission bands at 300 K appear in readable intensity and magnitude at 90 Hz in the middle-visible wavelength region (yellow region) at about 610 nm, and in the longer-visible wavelength region (orange-red region) at about 670 nm. In addition, a major spectral emission band at 77 K appears in readable intensity and magnitude at 9 Hz in the shorter-visible wavelength region (blue region) at about 470 nm.

The main termoluminescence (TL) glow curves are observed as the widest and highest bands peaked at nearly 95 ^{o}C at the end of the heating of 10 minutes, and at nearly 110 ^{o}C at the end of the heating of 30 minutes. These glow curves of Turkish purple jade, obviously, are different from the green and/or whitish colored jades from other regions in the world. This difference can be attributed to the formation conditions of the contact metamorphic aureole in the region, and it can be used to be one of the characteristic provenance identification methods for the Turkish purple jades.

REFERENCES

Adamo, I., Pavese, A., Prosperi, L., Diella, V., Ajò, D., Dapiaggi, M., Mora, C., Manavella, F., Salusso, F.,Giuliano. V., 2006. Characterization of omphacite jade from the Po Valley, Piedmont, Italy. *Journal of Gemmology, 30*, 215-226.

AMCSD, 2011. American Mineralogist crystal structure database by Downs et al. (1993), Retreived June 12, 2011, from http://www.minsocam.org/MSA/ Crystal_Database.html, and http://rruff.geo.arizona.edu/AMS/amcsd.php.

Andrews, E.W.V., 1986. "Olmec jades from Chacsinkin, Yucatan, and Maya ceramics from La Venta, Tabasco," in E. Wyllys Andrews V. (ed.), *Research and Reflections in Archaeology and History: Essays in Honor of Doris Stone* (New Orleans, LA: Tulane University, Middle American Research Institute).

Bersani, D., Lottici, P.P., 2008. Application of Raman spectroscopy to gemology. *Analytical and Bioanalytical Chemistry, 397*, 2631-2646.

Biino, G.G., Compagnoni, R., 1992. Very-high pressure metamorphism of the Brossasco coronite metagranite, southern Dora Maira Massif, Western Alps. *Schweiz Mineral. Petrogr. Mitt., 72*, 347-363.

Bingöl, E., Delaloye, M., Ataman, G., 1982, Granitic intrusions in western Anatolia: a contribution to the geodynamic study of this area. *Eclogae Geologica Helvatica, 75*, 437-446.

Bishop, C., Woolley, A., Kinnes, I., Harrison, R., 1977. Jadeite axes in Europe and the British Isles: An interim study. *Archaelogica Atlantica, 2*, 1-8.

Blasse, G., Grabmaier, B.C., 1994. Luminescent Materials. Springer–Verlag, 232.

Brizi, E., Mellini, M., 1992. Kinetical modelling of exsolution textures in igneous pyroxenes: *Acta Vulcanologica, 2*, 87-93.

Brothers, R.N., Grapes, R.H., 1989. Clastic lawsonite, glaucophane, and jadeite pyroxene in Franciscan metagraywackes from the Diablo Range, California. *Geological Society of America Bulletin, 101*, 14-26.

Cameron, M., Papike, J.J., 1981. Structural and chemical variations in pyroxenes. *American Mineralogist, 66*, 1-50.

Compagnoni, R., Maffeo, B., 1973. Jadeite-bearing metagranite and related rocks in Mount Mucrone area (Sesiap Lanzo Zone, Western Italian Alps). *Schweiz. Min. Petr. Mitt., 53*, 355-378.

Chihara, K., 1971. Mineralogy and paragenesis of jadeites from the Omi-Kotaki area, central Japan. *Mineralogical Society of Japan Special Paper, 1*, 147-156.

Chihara, K., 1991."Jade in Japan." in R. Keverne (ed.) *Jade* (New York: Van Nostrand Reinhold), 216-217.

Chihara, K., 1999. Jadeite in Japan. *Journal of the Gemmological Society of Japan. 20*, 5-21.

Coleman, R.G., 1961. Jadeite deposits of the Clear Creek area, New Idria district, San Benito County, *California. Journal of Petrology, 2*, 209-247.

Coleman, R.G., Lee, D.E., 1963. Glaucophane-bearing metamorphic rock types of the Cazadero area, California. *Journal of Petrology, 4*, 260-301.

Coleman, R.G., Clark, J.R., 1968. Pyroxenes in the blueschist facies of California. *American Journal of Science, 266*, 43-59.

Colomban, P., Prinsloo, L., 2009. *Optical spectroscopy of silicates and glasses. In; Yatwood, J, Douthwaite R, Duckett S.* (eds) Spectroscopic Properties of Inorganic and Organometallic Chemistry, RSC publishing, *40*, 128-149.

Crowhurst, D., 2001. Jade is jade. *Colored Stone, 14*, 112-113.

D'Amico, C., Campana, R., Felice, G., Ghedini, M., 1995. Eclogites and jades as prehistoric implements in Europe: A case of petrology applied to cultural heritage. *European Journal of Mineralogy, 7*, 29-41.

Delé-Dubois, M.L., Dhamelincourt, P., Poirot, J.P., Schubnel, H. J., 1986. Differentiation between gems and synthetic minerals by laser Raman microspectroscopy. *Journal of Molecular Structure. 143*, 135-138.

Easby, E. K., 1991. “Jade in South America and the Caribbean”, in R. Keverne (ed.) *Jade* New York: Van Nostrand Reinhold, 338-341.

Ernst, W.G., Banno, S., 1991. Neoblastic jadeitic pyroxene in Franciscan metagraywackes from Pacheco Pass, central Diablo Range, California, and implications for the inferred metamorphic *P-T* history. *New Zealand Journal of Geology and Geophysics, 34*, 285-292.

Essene, E., 1969. Relatively pure jadeite from a siliceous Corsican gneiss. *Earth and Planetary Science Letters, 5*, 270-272.

Fan, J.L., Guo, S.G., Liu, X.L., 2007. Application of Raman spectrometer (785 nm) to jadeite test (in Chine with English abstract), Retrieved March 8, 2011, from http://www.ncbi.nlm.nih.gov/pubmed/18306795.

Fan, J.L., Guo, S.G., Liu, X.L., 2009. The Application of confocal micro-Raman spectrometer to nondestructive identification of filled gemstones. *Spectroscopy Letters, 42*, 129-135.

Gaft, M., Reisfeld, R., Panczer, G., 2005. *Luminescence Spectroscopy of Minerals and Materials*, 1ed. Springer, Berlin, 456. ISBN-13-978-3-540-21818-7.

Gfroerer, T.H., 2000. Photoluminescence in analysis of surfaces and interfaces. In Encyclopaedia of Analytical Chemistry, R.A. Meyers (Ed.), John Wiley & Sons Ltd, Chichester, 9209–9231.

Garcia-Guinea, J., Correcher, V., Sanchez-Munoz, L., Finch, A.A., Hole, D.E., Townsend, P.D., 2007, On thermoluminescence emission band at 340 nm of stressed tectosilicate lattices. . *Nuclear Instruments and Methods in Physics Research Section B, 580*, 648–651.

Gendron, G., Smith, D.C., 2002. Gendron-Bdou, A. Discovery of Jadeite-Jade in Guatemala confirmed by non-destructive Raman microscopy. *Journal of Archaeological Science, 29*, 837–851.

Gouadec, G., Colomban, P., 2007. Raman Spectroscopy of nanomaterials: How spectra relate to disorder, particle size and mechanical properties. *Progress in Crystal Growth and Characterization of Materials. 53*, 1-56.

Götze J., 2000. Cathodoluminescence microscopy and spectroscopy in applied mineralogy. *Freiberger Foschungshefte*, 128-132.

Götze, J., Krbetschek, M.R., Havermann, D., Wolf, D., 2000. High-Resolution Cathodoluminescence Studies of Feldspar Minerals. In: Cathodoluminscence in Geosciences, pp.245.

Habermann, D., 2002. Quantitative cathodoluminescence (CL) spectroscopy of minerals: possibilities and limitations. *Mineralogy and Petrology, 76*, 247-259.

Handerson, B., Imbusch, G.F., 2006. Optical Spectroscopy. Oxford University Press, 672.

Hanni, H., Kiefert, L., Chalain, J.P., 1997. Raman spectroscopic applications to gemmology. *Journal of Gemmology, 25*, 394-407.

Harder, H., 1995. Trace elements as colouring agents in jadeites. *The Journal of Gemmology, 24*, 508-511.

Harlow, G.E., Sorensen, S.S., 2005. Jade (nephrite and jadeitite) and serpentinite: metasomatic connections. *International Geological Review, 47*, 113-146.

Harlow, G.E., Sorensen, S.S., Sisson, V.B., 2007. Jade. In: The Geology of Gem Deposits (ed., Lee A. Groat), Short Course Handbook Series 37, Mineralogical Association of Canada, Quebec, 207-254.

Hatipoğlu, M., 2010. Response to jadeite from Turkey. *Rocks & Minerals*, *85*, 301-301.

Htein W., Naing A.M., 1994. Mineral and chemical compositions of jadeite jade of Myanmar. *Journal of Gemmology, 24*, 269–276.

Kaya, O., Özkoçak, O., Lisenbee, A., 1989. Jura öncesi bloklu tortul kayaların stratigrafisi, Bursa güneyi). *Bulletin of MTA (Turkey), 109*, 22-32.

Krbetschek, M. R., Götze, J., Irmer, G., Rieser, U., Trautmann, T., 2002. The red luminescence emission of feldspar and its wavelength dependence on K, Na, Ca composition. *Mineralogy and Petrology, 76*, 167-177.

Lewis, I.R., Edwards, H.G.M., 2001. *Handbook of Raman Spectroscopy, From the Research Laboratory to the Process Line, Practical Spectroscopy Series,* Marcel Dekker Inc., New York.

Luff, B.J., Townsend, P.D., 1993. High sensitivity thermoluminescence spectrometer. *Measurement Science and Technology. 4*, 65-71.

Marshall, D.J., 1988. *Cathodoluminescence of geological material*. Unwin Hyman, Boston, 345.

Melo, A.P., Valerio, M.E.G., Caldas, L.V.E., 2004. Thermoluminescence characteristics of mineral samples acquired as jade. *Nuclear Instruments and Methods in Physics Research Section B, 218*, 198-201.

Middleton, A, Freestone, I., 1995. In: Rawson J (ed) *Chinese jade*. British Museum Press, London, 413.

Morimoto, N., 1988. Nomenclature of pyroxenes. *American Mineralogist. 73*, 1123-1133.

Morimoto, N., 1989. Nomenclature of pyroxenes. *The Canadian Mineralogist, 27*, 143-156.

Nassau, K., Shigley, J.E., 1987. A study of the general electric synthetic jadeite. *Gems & Gemology, 23*, 27-35.

Nestola, F., Tribaudino, M., Ballaran, T.B., Liebske, C., Bruno, M., 2007. The crystal structures of pyroxenes along the jadeite-hedenbergite and jadeite-aegirine joins, *American Mineralogist, 92*, 1492-1501.

Nutall, R.H.D., Weil, J.A., 1980. Two hydrogenic trapped-hole species in quartz. *Solid State Communications, 33*, 99-102.

Okay, A.I., 1980. Mineralogy, petrology and phase relations of glaucophane-lawsonite zone blueschists from the Tavşanlı region, northwest Turkey. *Contribution to Mineralogy and Petrology, 72*, 243-255.

Okay, A.I., 1984. Distribution and characteristics of the northwest Turkish blueschists. In: A.H.F. Robertson and J.E. Dixon (eds.) The Geological Evolution

of the Eastern Mediterranean, *Geological Society of London, Special Publication, 17*, 455-466.

Okay, A., Kelley, S.P., 1994. Tectonic setting, petrology and geochronology of jadeite +glaucophane and chloritoid +glaucophane schists from northwest Turkey. *Journal of Metamorphic Geology, 12*, 455–466.

Okay, A.I., 1997. Jadeite-K-feldspar rocks and jadeitites from northwest Turkey. *Mineralogical Magazine, 61*, 835-843.

Okay, A.I., Harris, N.B.W., Kelley, S., 1998. Blueschist exhumation along a Tethyan suture in northwest Turkey. *Tectonophysics, 285*, 275–299.

Okay, A.I., 2002. Jadeite–chloritoid–glaucophane–lawsonite blueschists in northwest Turkey: unusually high P/T ratios in continental crust. *Journal of Metamorphic Geology, 20*, 757-768.

Ponahlo, J., 1999. Cathodoluminescence du Jade. Revue de Gemmologie A.F.G., *137*, 10–16.

Prewitt, C.T., Burnham, C.W., 1966. The crystal structure of jadeite, $NaAlSi_2O_6$. *American Mineralogist, 51*, 956-975.

Raman, C.V., Krishnan, K.S., 1928. A new type of secondary radiation. *Nature, 121*, 501.

Rossman G.R., 1974. Lavender jade: The optical spectrum of Fe^{3+} and Fe^{2+}–Fe^{3+} inter-valence charge transfer in jadeite from Burma. *American Mineralogist, 59*, 868–870.

Rossi, G., Smith, D.C., Ungaretti, L., Domeneghetti, M.C., 1983. Crystal-chemistry and cation ordering in the system diopside-jadeite: a detailed study by crystal structure refinement. *Contributions to Mineralogy and Petrology, 83*, 247-258.

RRUFF, 2011. Database of Raman spectroscopy, X-ray diffraction and chemistry of minerals, Retrieved April 23, 2011, from http://rruff.info/. Department of Geosciences University of Arizona 1040 E 4th, Tucson, AZ, USA. 85721-0077

Sherlock, S., Kelley, S.P., Inger, S., Harris, N., Okay, A.I., 1999. 40Ar-39Ar and Rb-Sr geochronology of high-pressure metamorphism and exhumation history of the Tavşanlı Zone, NW Turkey. *Contributions to Mineralogy and Petrology, 137*, 46–58.

Slodczyk, A., Colomban, P., 2010. Probing the nanodomain origin and phase transition mechanisms in (un) poled PMN-PT single crystals and textured ceramics. *Material. 3*, 5007-5029.

Smith, D.C., Gendron, F., 1997. Archaeometric application of the Raman microscope to the non-destructive identification of two Pre-Columbian ceremonial polished "greenstone" axe heads from Mesoamerica. *Journal of Raman Spectroscopy. 28*, 731-738.

Smith, D.C., 2005. In: Edwards, H.G.M., Chalmers, J.M., (eds), *Raman spectroscopy in archaeology and art history*. RSC analytical spectroscopy monographs. Royal Society of Chemistry, Cambridge, 335–378.

Şengör, A.M.C., Yılmaz, Y., 1981. Tethyan evolution of Turkey: a plate tectonic approach. *Techtonophsics, 75*, 181-241.

Teixeira, M.I., Melo, A.P., Ferraz, G.M., Caldas, L.V.E, 2010. Application of jade samples for high dose dosimetry using the EPR technique. *Applied Radiation and Isotopes. 68*, 582–585.

Tuncer-Arslanlar, Y., Garcia-Guinea, J., Kibar, R, Çetin, A., Ayvacıklı, M., Can, N., 2011. Luminescence behaviour and Raman characterization of jade from Turkey. *Applied Radiation Isotopes, 69*, 1299-1306.

Townsend P.D., Rowlands A.P., 2000. *Information encoded in cathodoluminescence emission spectra*, in: M Pagel, V. Barbin, P. Planc, D. Ohnenstetter (Eds), ''Cathodoluminescence in Geosciences'', Springer Berlin, 41-57.

Zhao, Th., Yan, X.W., Cui, J., 1994. The physical and chemical properties of synthetic and natural jadeite for jewellery. *Journal of Material Sciences, 29*, 1514–1520.

Vandenabeele, P., 2010. Raman spectroscopy. *Analytical and Bioanalytical Chemistry, 397*, 2629–2630.

Vanoy, T.C., Levert A.M., McPherson, G.L., 1988. Luminescence spectra of crystals of RbMnCl3, Rb2MnCl4 and CsMnBr3 doped with Cr^{2+}: exciton trapping at luminescent Cr^{2+} centres. *Journal of Physics-C: Solid State Physics, 21*, 2969-2979.

WEBMINERAL, 2011. Minerals arranged by X-Ray powder diffraction, Retrieved June 13, 2011, from http://webmineral.com/MySQL/xray.php.

Weil, J.A., 1984. A review of electron spin spectroscopy and its application to the study of paramagnetic defects in crystalline quartz. *Physics and Chemistry of Minerals, 10*, 149-165.

Yılmaz, I.Ö., Altıner, D., Tekin, U.K., Tüysüz, O., Ocakoğlu, F., Açıkalın, S., 2010. Cenomanian–Turonian Oceanic Anoxic Event (OAE2) in the Sakarya Zone, northwestern Turkey: Sedimentological, cyclostratigraphic, and geochemical records. *Cretaceous Record, 31*, 207-226.